Giant Radio Galaxies

Edward Boyce

October 31, 2000

Abstract

Giant radio galaxies (GRGs) are the largest structures associated with single galaxies. Their linear sizes exceed 1 Mpc and so they form the extreme tail of the radio galaxy population. Because they have expanded to such large sizes, GRGs are thought to be the endpoint of radio galaxy evolution and provide important constraints to evolutionary models. They extend well past the environment of their host galaxy and act as direct probes of the intergalactic medium. I have carried out a survey for giant radio galaxies from a subset of the Sydney University Molonglo Sky Survey (SUMSS). My search area covered approximately $\sim$ 2100 square degrees, which corresponds to $\sim$26% of the area to be surveyed by SUMSS, or $\sim$5% of the sky. This is the most comprehensive southern sky GRG survey to date. I have identified twelve confirmed giants, a space density of one per 175 square degrees, and seventeen other candidate giants. The properties of these sources agree with a similar study in the northern hemisphere, and are consistent with theoretical models of the evolution of radio galaxies. Some interesting sources were found including: several double-double radio galaxies which show evidence of recurrent nuclear activity; some sources that may be the faded remnants of old radio galaxies; and J0331-771, perhaps the second largest radio galaxy known. A detailed investigation of one very powerful giant radio galaxy, J1919-799, revealed the processes at work in radio galaxies.

Acknowledgements

I would like to thank the following people for their contributions to this project:
My thesis supervisors, Richard Hunstead and Elaine Sadler, assisted me at all stages of the project and helped to define its scope. They gave step by step guidance in all aspects of the work, including giant source identifications, measurement techniques, making optical identifications, interpretation and reporting of the project.
Richard Hunstead took some of the Australia Telescope observations of the source J1919-799, wrote the observing proposal for the optical spectroscopy and performed some of the spectroscopic data reduction.
Ravi Subrahmanyan took some of the Australia Telescope Observations of J1919-799, reduced the 5.8GHz data for this source and taught me to use the Miriad package to reduce the other frequencies.
Vince McIntyre reduced the Australia Telescope data for J0331-771, and often helped with computing difficulties.
Elaine Sadler, Vince McIntyre, Carole Jackson, Richard Hunstead and Anne Green submitted the proposal for the Australia Telescope observations of J0331-771.
Ann Burgess provided data used in deriving the method of estimating redshifts from b_J magnitudes.
Raylee Stathakis performed the spectroscopic observations at the Anglo Australian Observatory.
This project used data from the ROE/NRL COSMOS UKST Southern Sky Object Catalog.

I certify that this Thesis contains work carried out by myself except where otherwise acknowledged.

_____ Date: _____

Contents

Chapter 1

Introduction

Giant radio galaxies are the largest single structures in the universe. They are interesting as rare extreme sources in the radio galaxy continuum and as probes of intergalactic space. This project is a survey of these objects from SUMSS (Sydney University Molonglo Sky Survey).

1.1 Radio Galaxies

1.1.1 Structure of Radio Galaxies

When radio astronomers look at radio emission from the sky, the brightest structures they see are the radio galaxies. These are linear double structures - two diffuse regions of radio emission, called lobes, which lie either side of a host optical galaxy. At high resolution smaller and brighter structures become apparent. A very small, bright core is often seen between the lobes, coinciding with the host galaxy. Straight, narrow jets are often seen connecting the core to one or both lobes. Where a jet reaches the end of the lobes there is usually a hotspot - a small region of more intense emission on the outer edge of the lobe. In Figure 1.1.1 these features are illustrated for Cygnus A, the prototypical radio galaxy.

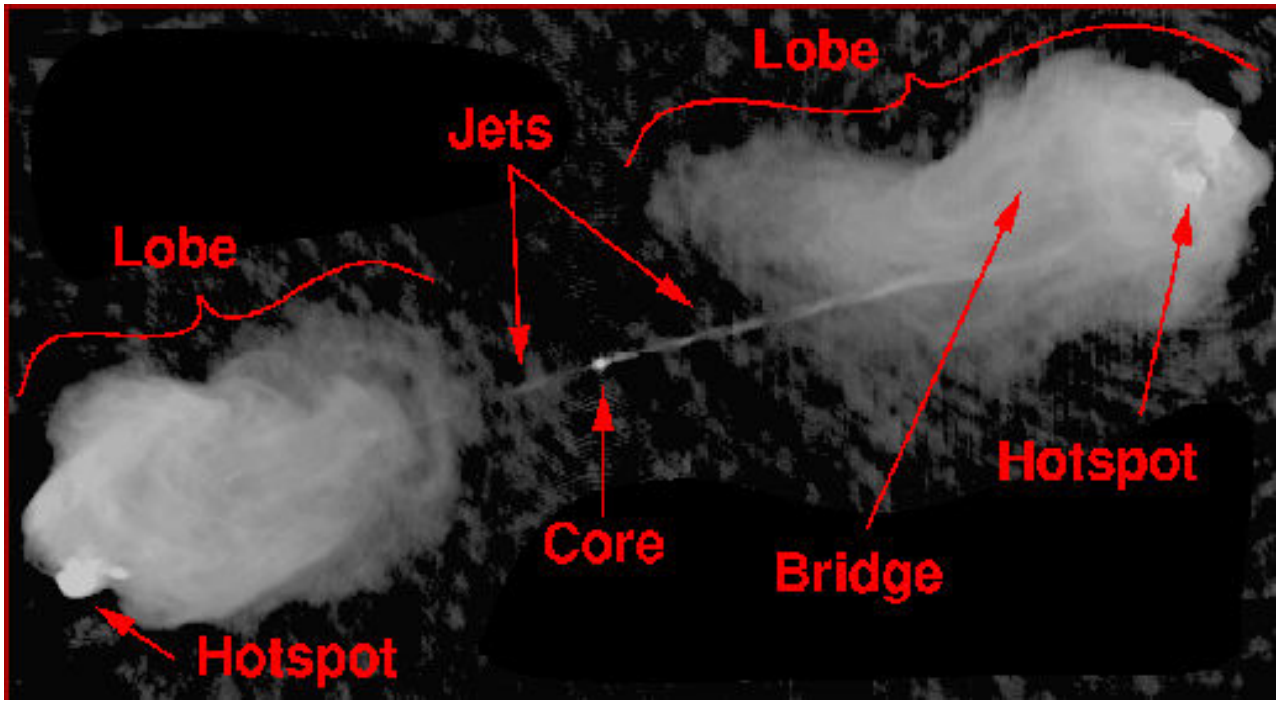

Figure 1.1: Cygnus A, with main radio galaxy structures labelled (Leahy et al., 1999).

Double sources are divided into two types, the Fanaroff-Riley classes (FRI and FRII), based on the brightness distribution within their lobes (De Young, 1976). FRI sources are edge-darkened, with the central

section having a higher radio flux density than the outer edges of the lobes. FRII sources are edge-brightened, with the outer edges of the lobes having higher flux density than the inner regions. Depending on the flux density limit of an observation the inner regions of an FRII source may not be visible. In general, FRII sources have a higher luminosity (total power of radio emission) (Fanaroff & Riley, 1974).

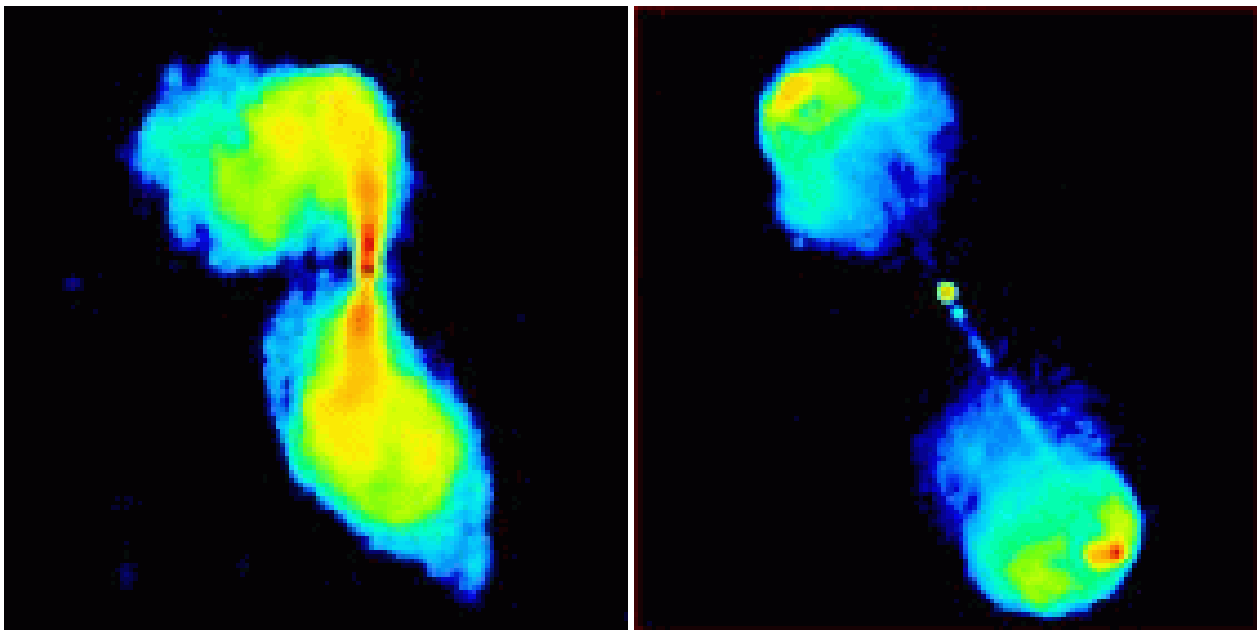

Figure 1.2: An FRI radio galaxy, 3C272.1 (left) (Laing & Bridle, 1987) and an FRII radio galaxy, 3C47 (right) (Leahy, 1996).

1.1.2 Formation of Radio Galaxies

The spectrum of the radio emission from the lobes indicates that it is synchrotron radiation, generated by energetic electrons moving in a magnetic field. We therefore conclude that radio galaxy structures are composed of magnetised relativistic plasma. Synchrotron emitting electrons lose energy rapidly and so there must be a source of high energy electrons. As no objects are observed in the radio lobes other than the plasma itself, the protons and electrons must originate in the host galaxy.

In the standard twin-beam model for radio galaxy formation (De Young, 1976) two jets of particles are formed in the central region of the host, known as the Active Galactic Nucleus (AGN). The AGN is seen as the small radio core, but is so small that it is usually unresolved. This small angular scale, and intervening dust, means that the details of the initial jet formation have not been observed, and the models have not been rigourously tested. The most likely explanation involves a supermassive black hole located in the AGN. Particles from the black hole's accretion disk are collimated into two oppositely directed relativistic beams. These beams become the jets, which stream outwards and carry highly energetic particles into the lobes.

The subsequent behaviour of the jet differs depending on the radio morphology. In FRI sources the jet soon changes direction and loses energy, and does not reach the edges of the lobes. For FRII sources the jet moves in almost a straight line through the lobes, bending slightly due to perturbations from magnetic fields and density variations. When the jet reaches the end of the lobe it encounters the intergalactic medium (IGM) and forms a plasma shock. The jet stops and mixes with the IGM, releasing considerable kinetic energy. Some of the energy is radiated away and seen as the bright hotspot, while some accelerates the particle thermal speeds to relativistic levels. The continuous pressure of the jet steadily pushes the shock front away from the optical galaxy, leaving behind relativistic plasma which spreads out behind it. The advancing jets inflate a cocoon of energetic plasma within the IGM, seen as a radio lobe. After 10^7 – 10^8 years the AGN stops producing the jet, leaving a fading, slowly expanding remnant lobe.

The luminosity gap between FRI and FRII radio galaxies indicates that the jets transport more energy into the radio lobes for FRII galaxies. This is thought to be due to variations in the jet speed. The faster FRII

jets remain laminar while traversing the whole lobe and form a hotspot when they meet the IGM. The slower FRI jets become turbulent in the lobes and deposit most of their energy within the lobes. The difference in jet power may be caused by lower initial jet powers for the FR I sources. (Kaiser & Alexander, 1997), or by higher matter density just beyond the AGN in FRI sources, which slows the jets down.

1.1.3 Spectral Ageing in Radio Galaxies

Support for the twin beam model comes from measurements of spectral ageing. The radiation flux, S, from a radio galaxy follows a power-law distribution characteristic of synchrotron emission, $S_\nu \propto \nu^\alpha$, where α is the spectral index. As the electrons radiate away energy their synchrotron emission shifts to lower frequencies and the spectrum steepens. Measurements of α can thus be used to determine the time since the plasma was formed. The spectral index is flattest in the hotspot regions, flat at the edges of the radio sources and steepens towards the inner edge of the lobes. This is consistent with high-speed jets transporting plasma from the core and forming relativistic electrons at a shock region. As the shock moves away the plasma left behind in the lobe loses energy and α steepens. Regions nearer to the core were formed earlier, and so they have lost more energy and have steeper spectra.

There are more detailed models to estimate the exact age of a lobe region from the radiation spectrum. These include other factors which change the radiation spectrum, such as inverse Compton scattering of microwave background photons, the pitch angle distribution of the relativistic electrons and a finite lifetime for the particle beams (see Komissarov & Gubanov 1994; Mack et al. 1998).

1.2 What makes a Radio Galaxy a Giant?

The largest single galaxy structures in the universe, which form the subject of this thesis, are the giant radio galaxies (GRGs). A radio galaxy is classified as a giant if its projected linear size is greater than or equal to a megaparsec (Mpc). Since the definition relies on projected linear size, the classification of a source as a giant depends on its orientation.

There is an additional ambiguity, since the derivation of a source's projected size from its angular size and redshift relies on cosmological assumptions. One must use values for the matter density of the universe, Ω_m, the cosmological constant Ω_Λ, and the Hubble constant H_0. Most GRG authors (e.g. Ishwara-Chandra & Saikia, 1999; Schoenmakers, 1999; Subrahmanyan et al., 1996) assume $\Omega_m = 1$, $\Omega_\Lambda = 0$ and $H_0 = 50$ $kms^{-1}Mpc^{-1}$. The latest cosmological measurements indicate that this model is inaccurate (Turner, 1999; Lineweaver, 1999).

In this thesis I have mostly worked with the old model, which makes it straightforward to compare my results with previous work on giant sources. See Section 3.5 for a fuller discussion.

1.3 Properties of GRGs

The two largest surveys of GRGs to date are those of Ishwara-Chandra & Saikia (1999) and Schoenmakers (1999). Most of the conclusions about GRG properties are drawn from these surveys. See Section 1.7.4 for a discussion of the selection effects in the Schoenmakers survey.

Figure 1.3 shows the P-D diagram for the Ishwara-Chandra & Saikia survey, with GRGs shown alongside uniform samples of all sources. A P-D diagram plots the total power ouput from all the radio emission across the galaxy against its linear size. One notable feature of the diagram is a lack of giant sources with high radio powers. Unlike the sample of all sources, there is a cutoff in radio powers at $\sim 3 \times 10^{27}$ W. There is also a dropoff in linear size at $\sim$3 Mpc, with only one source (3C 236) exceeding 3 Mpc.

It should be noted that the powers of the giants are similar to the middle range of powers for smaller sources, but their lobes cover a larger area. This reflects the structure of the giants, which have lobes with a lower surface brightness than smaller sources but extending over a larger area. With such diffuse emission the brightness levels are often similar across the source. Ishwara-Chandra & Saikia (1999) found that most giant sources are FRII, but many lie near the transition region between FRI and FRII.

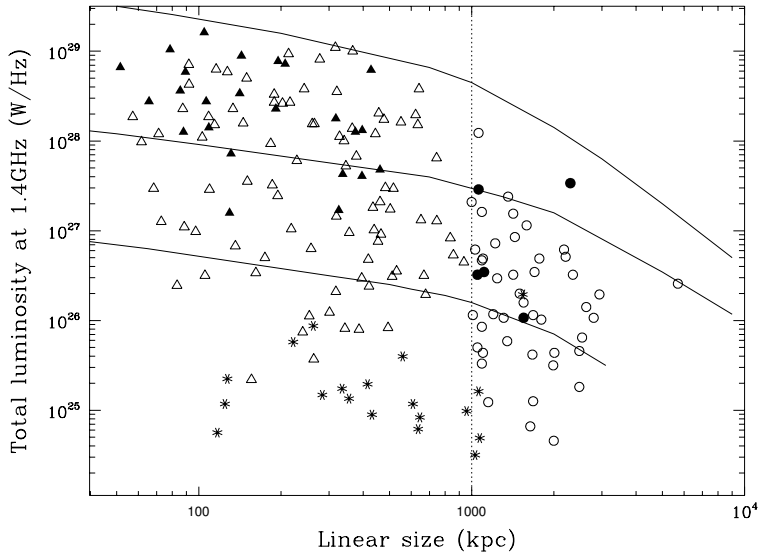

Figure 1.3: Ishwara-Chandra & Saikia's sample of GRGs (circles), plotted with the 3C Radio Galaxy Catalog (triangles) (Ishwara-Chandra & Saikia, 1999a). Filled symbols are for sources associated with quasars and open symbols are for sources associated with active galaxies. The asterisks are FRI sources, all other sources have FRII morphology. Note that virtually all of the giant sources are FRII radio galaxies. The lines plotted are theoretical evolutionary tracks for three jet powers (see Section 1.4.)

Schoenmakers (1999) uses spectral index measurements of the lobes to show that the giant source lobes are on average 8×10^7 years (80 Myr) old. This is older than smaller radio sources, but not by much.

1.4 Formation of GRGs

Giant radio galaxies are immense structures, larger than small groups of galaxies. Our own local group is only 2.4 Mpc across (van der Bergh, 1999), while many GRGs have a *projected* size between 2 and 3 Mpc. The most obvious motivation for the study of the giants is to understand the physical processes that generate a coherent structure over such large distances.

In existing models (Kaiser et al., 1997), the giant sources are the end stage of a radio galaxy's evolution. The galaxy starts out as a compact source less than 10 kiloparsecs (kpc) across, smaller than the host galaxy. As the jets expand and start to inflate a radio lobe the source changes to a standard FRI or FRII radio galaxy, depending on the jet power. At some point the jets shut down and as the electrons gradually lose energy the radio power declines while the lobes continue to expand. The source traces out a line moving down and to the right in the P-D diagram (see Figure 1.3). After $\sim10^7$ years the source may have expanded enough to become a giant. The loss of energy in the ageing lobes explains the energy cutoff in giant sources, while the lack of sources larger than 3 Mpc corresponds to the typical size cocoon which the jets can inflate before the central source closes down.

This theory is very general and many details need to be filled in and checked. It is not known what proportion of FRI and FRII sources go on to be giants, and what factors influence the likelihood of such an evolution. The ages of giants are not much greater than those of small sources, which indicates that other factors may have an influence. The tendency for giants to be FRII may indicate that high initial powers are needed to generate a 1 Mpc lobe. However, it could be that this is a selection effect. FRI sources are less powerful initially and as they lose power with age, their lobes become difficult to detect. The Ishwara-Chandra & Saikia sample relies on GRGs in the literature. Such GRGs are generally chance discoveries in other, flux-limited samples and so they will tend to have high fluxes and high radio powers.

Another possibility is that the intergalactic medium is less dense in the vicinity of a giant, as outlined in the next section. The IGM density and pressure should decrease with time as the universe expands. If giant formation does depend strongly on ambient pressure we should see fewer such sources at higher redshifts (which correspond to earlier cosmological epochs). Giant frequencies may also indicate when the era of

reheating occurred, since this would boost the IGM pressure.

1.5 A Probe for the Interstellar Medium?

The jets and lobes of a giant radio galaxy extend well past the gaseous halo of the parent galaxy into the intergalactic medium. The jets and lobes are clearly interacting with this material, allowing it to be studied in some detail. Of particular interest is the pressure within the lobes, well away from the hotspots and any intense emission associated with bends in the jets. The pressure P is given by P = (1/3)u_{eq} (Schoenmakers, 1999), where u_{eq} is the equipartition energy density (the energy density assuming energy is evenly divided between particles and magnetic fields). u_{eq} can be calculated from the luminosity, volume and spectral index (Mack et al., 1998).

Subrahmanyan & Saripalli (1993) find that the lobes of giant radio galaxies all have pressures in the range 1-3$\times 10^{-15}$ Pa. The consistency of the pressure for sources of differing size suggests that they are in pressure equilibrium with a fairly uniform IGM. There is even a suggestion that the pressure increases weakly with redshift (which is consistent with the IGM density decreasing as the universe ages and expands). However, this result was derived from only eight sources and may not be reliable.

Schoenmakers (1999) mapped the pressure distribution across the lobes, and found that a pressure gradient from high near the hotspots to low near the core, showing that the lobes are not in equilibrium. Since the lobe pressure cannot be less than IGM pressure (otherwise the lobe would not inflate), the lobe pressure exceeds the IGM pressure. Hence Schoenmakers' own lobe pressures of 2-40$\times 10^{-15}$ Pa do not constrain the IGM pressure.

The other means of constraining IGM pressure is by measuring the advance speeds of the hotspots from the spectral ages of the hotspots and material in the lobes behind. This can be converted to a jet pressure, which must be balanced by ram-pressure from the IGM in front of it. Using this method both Schoenmakers (1999) and Mack et al. (1998) find that the IGM particle density lies between 10^{-11} and 10^{-10} m^{-3}, corresponding to a pressure of $\sim 2\times 10^{-15}$ Pa. The IGM densities derived by these researchers are lower than for smaller sources by a factor of about ten, suggesting that a low density region in the IGM assists in the formation of GRGs.

1.6 Double-Double Sources

An unusual class of objects has been detected in the Schoenmakers (1999) sample and has been the subject of several follow-up papers. Tentatively named double-double radio galaxies (DDRGs) these are FRII radio galaxies with two large lobes and two small, compact lobes embedded in the larger ones (see Figure 1.6). While DDRGs need not be giants, many are larger than 1 Mpc, and any survey of giant sources should turn up some double-doubles.

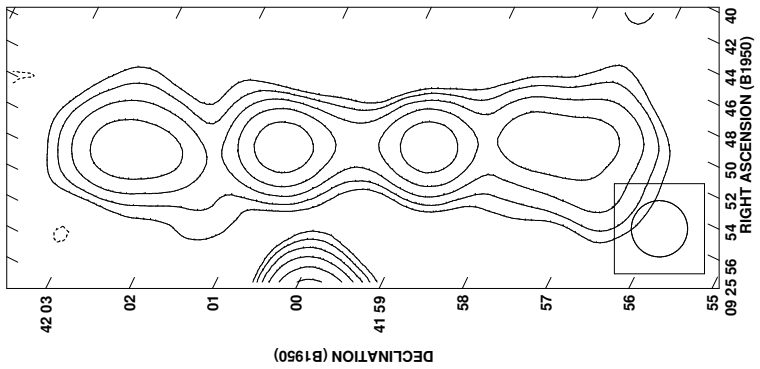

Figure 1.4: The double-double radio galaxy J0925+420 (Schoenmakers, 1999). 1.4 GHz contours from the NVSS (a survey made by the Very Large Array), set at -1.3, 1.3, 2.6, 5.2, 10.4, 20.8, 41.6 mJy/beam

The structure suggests repeated episodes of AGN activity. The AGN switches on, generates a jet for $\sim 10^7$ years and the jet forms a lobe. The AGN then switches off, while the lobe spreads out and fades. The

AGN then switches on again, generating new jets which inflate a new, smaller lobe, within the cocoon of the old one. There are difficulties with this theory, as the lobe is thought to have a lower density than the IGM, making the formation of a new lobe within it unlikely, although new models may alleviate this difficulty. The discovery and study of more DDRGs should farther the understanding of AGN activity and possible cycles within it.

1.7 Selection Effects and Complete Samples

The study of any group of astronomical objects is complicated by selection effects. Astronomical instruments are more sensitive to sources with higher integrated flux (brightness) and higher flux density (surface brightness). Sources which have higher brightness or surface brightness will appear more frequently in any survey, distorting the statistical properties of the objects included. The three most glaring selection effects in any GRG survey are the exclusion of fainter sources at high redshift (Malmquist bias) the exclusion of sources near the 1 Mpc size limit at high redshift, and the exclusion of sources with low surface brightness and steep spectra.

1.7.1 Malmquist Bias

A survey detects only sources with a flux greater than some limit - sources are excluded below this cutoff. For a given intrinsic power (power generated at the source) the observed flux decreases with increasing redshift, and will eventually fall below the cutoff. As redshift increases more low power sources are excluded but the high power sources are still observed. The high powered sources are rare and at high redshift, which corresponds to sampling from a larger volume, more high power sources will be observed. Thus the average power seems to increase with increasing redshift (see Figure 1.7.1). One should always keep in mind that a survey will be biased towards high powered sources at high redshifts.

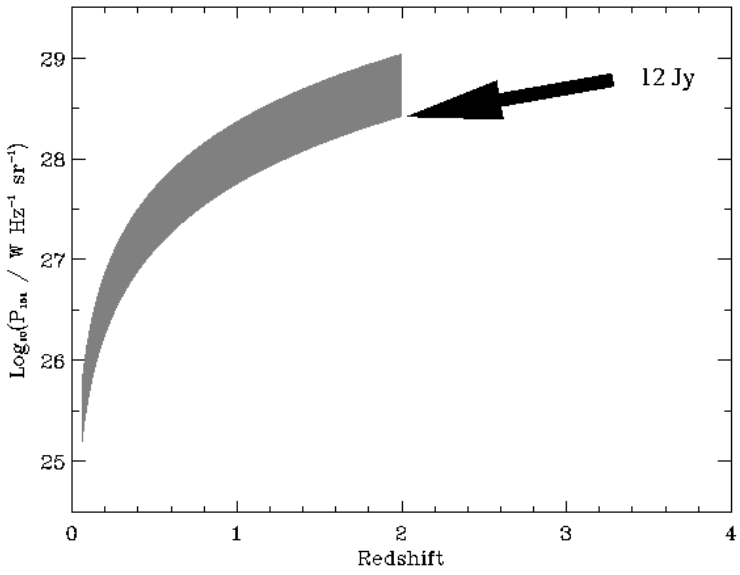

Figure 1.5: The shaded regions marks the powers observable at different redshifts for the 3C sample of radio galaxies. The lower line marks the smallest observable power due to a 12 Jy flux limit, the upper line marks the highest power observed at that redshift. At high redshift the sample covers a larger volume, so more of the rare high power sources are included (Blundell et al., 1999).

1.7.2 Linear Size Bias

In selecting candidate GRG sources it is necessary to look for sources with angular sizes above some given cutoff. However, a given angular size corresponds to a larger linear size at higher redshift. For a sufficiently

high redshift a source with a projected size greater than 1 Mpc may fall beneath the cutoff. Figure 1.6 shows the linear size corresponding to an angular size of 5 arcminutes (the size used in the Schoenmakers survey) for selected redshifts. for GRGs. Clearly any angular size cutoff will exclude some GRGs for redshifts greater than $\sim$0.15. This effect complicates the study of how GRG sizes evolve with redshift, since only the larger GRGs will be included at high redshift. Size evolution results will be most accurate for low redshifts, when we can be sure that all 1 Mpc sources have been included.

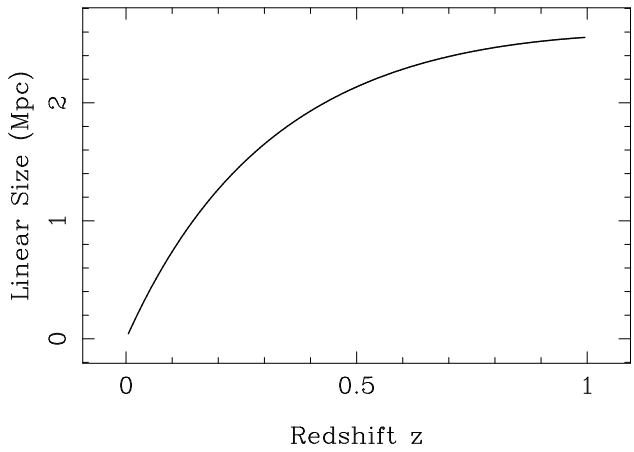

Figure 1.6: Linear Size of a 5 arcminute source over a range of redshifts, assuming Ω_m = 1.0, Ω_Λ = 0 and H_0 = 50 $\mathrm{kms}^{-1}\mathrm{Mpc}^{-1}$.

1.7.3 Surface Brightness and Frequency

Radio interferometers are sensitive to small bright regions, not large diffuse regions. The lobes of a GRG generally have a low surface brightness, as they are spread over a large area of sky. Instruments with long minimum baselines (such as the VLA and ATCA) are not good at detecting these large, diffuse sources, and will exclude many giant sources with fluxes that should be detectable. Therefore, it is desirable to look for giants with a telescope that has a short minimum baseline.

Moreover the plasma in the lobes is very old and will have a steep spectral index dominated by low frequencies. This low-frequency emission is hard to observe at frequencies of 1.4 GHz or higher.

1.7.4 Uniform Surveys

The two largest surveys of GRGs to date are those of Schoenmakers (1999) and Ishwara-Chandra & Saikia (1999). The Ishwara-Chandra & Saikia survey draws together 53 known GRGs from the literature. Some were taken from samples with differing selection criteria, but most were single-source analyses. Since their sources were taken with many different instruments with differing sensitivities, the combined biases are hard to estimate.

The Schoenmakers survey consists of 47 sources drawn from the Westerbork Northern Sky Survey (WENSS). This is a single sky survey by one instrument, the Westerbork Telescope. It has minimum baselines down to 36m and observes at the low frequency of 325 MHz. so WENSS can see large faint low-frequency structures rather well. There are well defined selection biases, with the size cutoff rising above 1 Mpc when for $z > 0.146$. There are also well-defined power cutoffs.

The Sydney University Molonglo Sky Survey (SUMSS) is a similar survey to WENSS in the southern sky. The Molonglo Observatory Synthesis Telescope (MOST) has a short minimum baseline of 4.4m and an observing frequency of 843 MHz, making it sensitive to the low surface brightness and low frequency of the GRGs (see Bock et al., 1999). This makes MOST suitable for a uniformly selected survey in the southern hemisphere comparable to Schoenmakers' survey in the north.

Chapter 2

Identifying the Galaxies

29 candidate giant radio galaxies were found by scanning a subsection of the SUMSS fields covering ∼2100 square degrees, or ∼5% of the sky. The radio properties of the sources were measured and optical images were used to search for the optical counterparts to the radio galaxies. Of the 29 candidates which met the angular size criterion, optical identifications were made for 15 and tentative optical identifications were made for nine more.

2.1 Selecting Sources from SUMSS

2.1.1 Field Selection

SUMSS is a radio survey of the southern sky at declinations south of -30°. The survey consists of 12 hour observations by MOST at its observing frequency of 843 MHz, which result in elliptical sky fields extending 2.7° in right ascension and 2.7 cosec(δ)$^\circ$ in declination. 2713 such fields will be observed over the course of the survey; 35% had been completed as of February 2000. The fields overlap and are combined into $4^\circ \times 4^\circ$ mosaics, which reduces the signal to noise.

The survey is incomplete and many fields have not yet been combined into mosaics. To increase the area of sky covered in the GRG search it was necessary to scan the individual fields, not the finished mosaics. The search process involved making a visual scan of the printed greyscale images of fields from the SUMSS archive. The search was made using all fields observed up to 29th February, 2000 which had declinations $\delta < -50^\circ$ and galactic latitude $|\mathrm{b}| > 12.5^\circ$.

The declination cutoff was necessary to reduce the noise levels; the fields become noisier at northerly declinations, as shown in Figure 2.1. The MOST beam is steered in the north-south direction by mechanically rotating the array and in the east-west direction by incorporating differential phase delays in the feeds. This process reduces the collecting area and hence the signal to noise ratio for observations at large distances from the meridian. More northern SUMSS fields incorporate observations from larger meridian distances; hence the signal to noise ratio is lower at northern declinations. The noise is particularly bad at the field edges and the mosaics are formed from the central regions, so the field noise does not affect the mosaics as much as Figure 2.1 might suggest. However, the noise was a problem for this search, which had to be done on the fields. Extended low surface brightness structure from a giant radio galaxy is lost in the noise and hence the identification of a GRG becomes ambiguous. For this reason the search was restricted to far southern fields, at declinations $\delta < -50^\circ$.

An essential part of the project is finding optical counterparts; detecting the host galaxies in visible light. Because giant sources are rare, they tend to be distant and so their host galaxies are faint and can be difficult to distinguish from stars. Near the plane of the galaxy the star density is high and the optical fields become very crowded. It is difficult to assign a unique identification to a radio galaxy; there will be many objects between the lobes which could plausibly be the host. Similarly the Magellanic Clouds contain regions of radio emission which look like radio galaxy lobes and confuse the radio fields. To keep the radio and optical identifications reasonably free of confusion the only sources included were those with galactic latitude $|\mathrm{b}| > 12.5^\circ$ (following Schoenmakers, 1999) and which did not coincide with the Magellanic Clouds. To allow for off-centre sources I looked at fields with centres at galactic latitudes $|\mathrm{b}| > 11^\circ$.

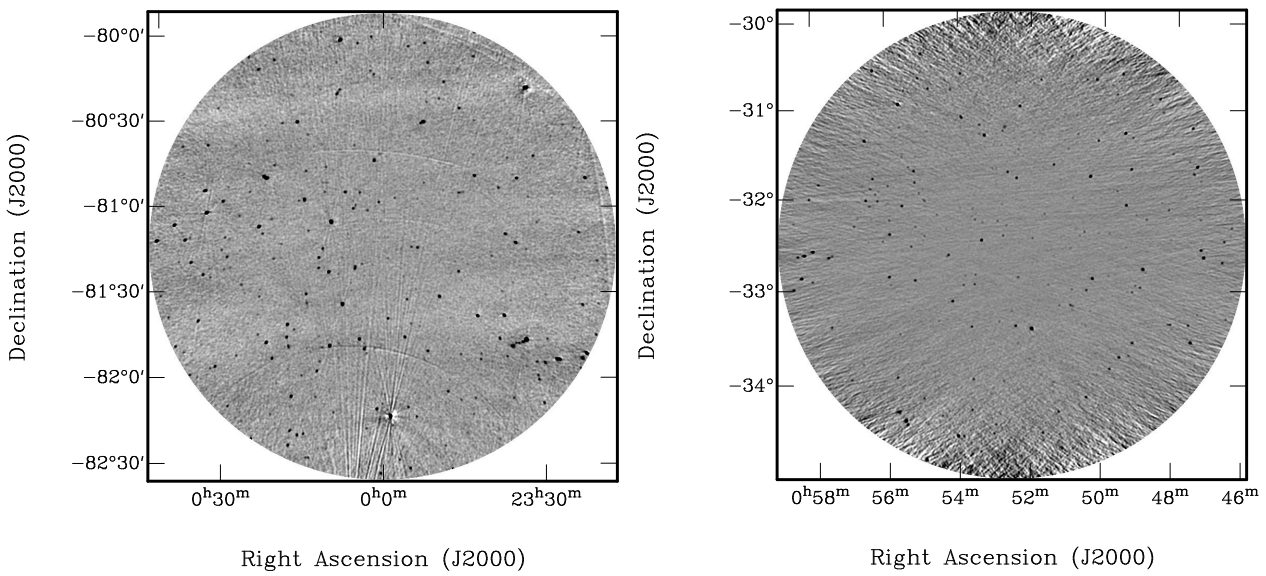

Figure 2.1: (left) A southern SUMSS field. (right) A higher noise northern field. The image lookup table and intensity scale are the same for both images. Only the central region of the northern fields is used in the mosaics, but the noisy edge region does make the northern fields less useful as individual fields.

In total, 425 individual SUMSS fields were searched. Allowing for the overlap between fields, the effective area of each field is ∼5 square degrees and so the area surveyed is ∼2100 square degrees. This area covers ∼5% of the sky and ∼26% of the region to be surveyed by SUMSS.

2.1.2 Criteria for Source Selection

When scanning the printed greyscale images I looked for any single structure at least 5 arcminutes in length (again following Schoenmakers 1999). This offers a compromise between finding most sources with linear sizes greater than 1 Mpc, and not having to deal with too many sources. I looked for single connected structures, double sources which appeared to be extended towards each other, and any triple sources. Sources which appeared to meet the criteria were included in the list of candidates.

The sources can only be considered candidates at this stage, since they could be a chance alignment of two or three extended sources. Confirmation of the connectedness of the sources would require high resolution radio images, to detect the presence of the classic radio galaxy structures such as a core, hotspots and jets.

Two sources were found which were more than 5 arcminutes across, but which were known head-tail sources from previous survey. Since head-tails are a different class of object to the giants, these two interlopers were not included in the list. They are discussed in Section 6.1.

2.2 Measuring Radio Properties

2.2.1 Radio Flux Density

The total flux density was measured using the imaging program `kview`. I selected rectangular regions that appeared to include the source and the main sidelobes, and took the integrated flux density over this region. If the region contained unrelated sources, then I measured the integrated flux density in a box around these sources, and subtracted it from the total. The flux density was measured over a region because the large and irregular structure of the radio lobes could not be modelled as an elliptical gaussian, and a source fitting program would return erroneous results.

Within the region defined by the flux fitting box but excluding the unrelated source boxes, I measured the centroid of the source using the routine `imom` from the image processing and analysis program Miriad. The centroid was used to locate optical hosts (see Section 2.4). and to assign names to the sources. The usual

practice is to name the source after its optical identification, but I did not have optical identifications for all my sources and so I used the centroids instead.

The peak flux density in each lobe was measured using the Miriad routine `maxfit`, which fits a quadratic to a three pixel by three pixel box, adjacent to the peak pixel. The peak is generally at the edge of an extended lobe. This extended emission on one side of the peak pixel means that a source fitting program which attempted to fit an elliptical gaussian would return incorrect results. `maxfit` operates only over a three by three pixel box, so it is largely insensitive to the extended emission, and just corrects for the peak emission not exactly coinciding with the peak pixel.

2.2.2 Angular Size

Giant radio galaxies have an FRII morphology (see Section 1.1.1) and the standard definition of their size is the angular separation between the hotspots at the edges of the source. These positions are best measured from a high resolution radio images at a frequency of 1.4 GHz or higher. MOST has a large beamwidth of $43\times43\cos\delta$ arcseconds and observes at 843 MHz, where spectral ageing makes the inner regions of the lobes are relatively brighter. The large beam blurs together the hotspots, which do not stand out so strongly from the lobe, and puts the peak inside the actual location of the hotspots, as shown in Figure 2.2. Therefore, measuring the distance between the MOST peaks underestimates the true angular size.

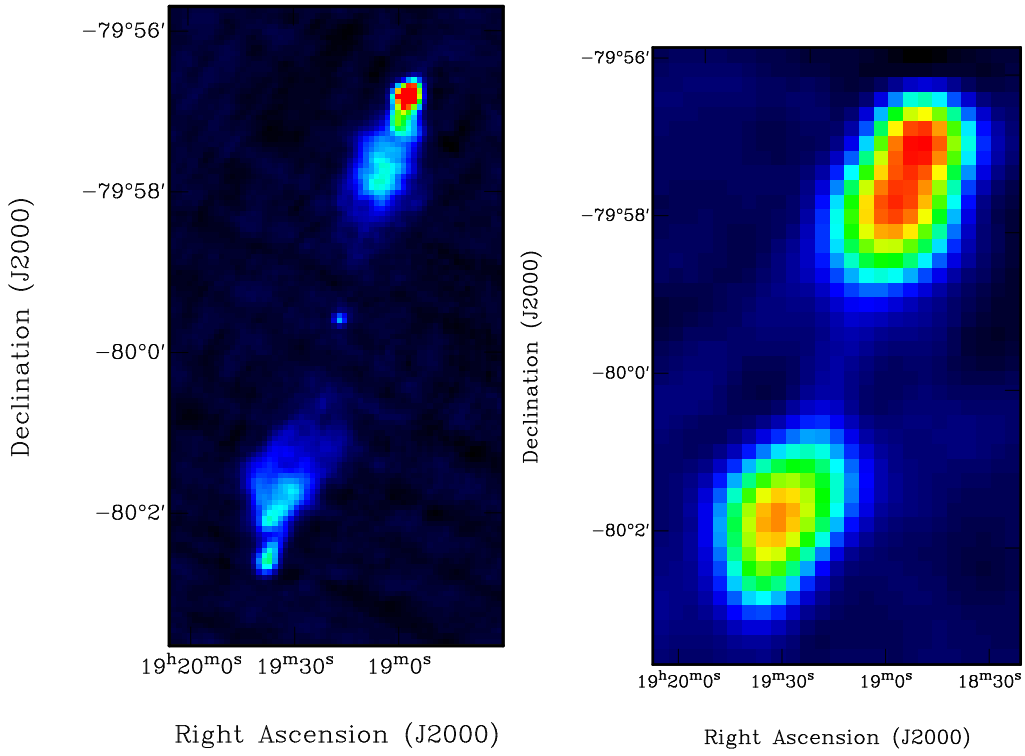

Figure 2.2: J1919-799. (left) High resolution 1.4 GHz observation from the Australia Telescope. (right) Lower resolution 843 MHz observation from SUMSS. The SUMSS peaks are shifted inwards from the hotspots, particularly in the southern lobe.

To correct the MOST errors, I compared the angular size discrepancies between MOST and high resolution images for eight giant sources. These giants, taken from a pre-SUMSS survey of MOST extended sources (Jones & McAdam, 1992), were the subject of a detailed study with the Australia Telescope Compact Array (Subrahmanyan et al., 1996). The ATCA 1.4 GHz data allowed the detection of hotspots and accurate measurements of total angular size. I measured the MOST peak to peak separations for the eight giants, and found that the hotspot to hotspot separation was between 1 and 1.32 times the MOST peak to peak distance. On average the true angular size was 1.14 times that measured by MOST.

In view of this result, the angular size of a source in this survey was taken to be the MOST peak to peak angular size, multiplied by 1.14. Since the true ratio of hotspot to hotspot separation to MOST peak

to peak separation varies by up to 10%, there is a 10% uncertainty in this multiplication factor and hence an uncertainty of ∼10% in the corrected angular size.

Some sources which were initially selected from the greyscale plots had angular sizes less than 5 arcminutes, even after the correction. These sources are listed in Table B.1 but are flagged since they do not meet the selection criteria. They are not included in any subsequent listing or graph of the sources dealing with physical properties. In all, 29 sources were found which appeared to be connected structures with angular sizes of at least 5 arcminutes.

2.3 Sensitivity Limits

The selection of sources is always limited by the sensitivity of the telescope. To be selected as a giant from the greyscale fields the source needs to have a flux density exceeding the noise over a considerable portion of its angular extent. If the emission is too faint then the source will not appear as a connected structure.

This limit on source detection is usually expressed in terms of the source's surface brightness, which is the integrated flux density divided by area. For a linear radio galaxy observed with a large beam radio telescope the source will be roughly one beam width wide regardless, regardless of length. The number of beams in which the emission is contained will be roughly proportional to the angular size of the source, and this number of beams gives the effective area over which the integrated flux must stand out from the noise. Schoenmakers argues that for a giant source, the integrated signal to noise $(S/N)_{int}$ is proportional to the integrated flux, S_{int}, divided by the angular size, θ (Schoenmakers, 1999), and uses the ratio of S_{int} to θ to define the observational limits of his sample. So I will define the sensitivity parameter Σ by:

$$\Sigma = \frac{S_{int}}{\theta} \tag{2.1}$$

and use this quantity to derive observational limits for my sample. While not the surface brightness, Σ is closely related to it and seems to be a useful measure of sensitivity for giant sources.

Figure 2.3 shows the sensitivity parameter defined by equation 2.1, plotted against angular size for all sources. It can be seen that the detection rate drops off below 20 mJy/arcmin, and we may set 17 mJy/arcmin as a practical lower limit on Σ. The exact value is somewhat arbitrary; this is only a rough minimum below which a source is unlikely to be detected. The minimum value of the sensitivity parameter constrains the physical properties of observable sources (see Section 3.3).

Note that two sources fall below this minimum. Both have a low ratio of total flux density to angular size because they consist of multiple components which are individually bright but with no detectable emission between them. They were selected as connected structures because the components had a high degree of symmetry, suggesting a common origin. J2159-723 ((S_{int}/θ) ∼13.5), has a good optical identification, shows a classic double-double morphology (see Section 4.4 for more details) and is almost certainly a single source. J0745-775 ((S_{int}/θ) ∼9) is probably not a single source, and is discussed fully in Section 3.3.1.

2.4 Making Optical Identifications

To determine the physical parameters of the giant sources, it was necessary to find their host galaxies. I searched for the galaxies by overlaying SUMSS contours of the candidate giant sources on greyscale optical images of the Digitised Sky Survey (DSS). These plots are shown in Appendix C. If there appeared to be an optical object in the appropriate location then I checked online databases to be sure that the object was a galaxy and not a star. The blue magnitudes b_J were all taken from the COSMOS database.

Host galaxies contain the active galactic nucleus (AGN) and so they coincide with the core of the radio galaxy. If a high resolution observation shows the core, then one simply looks on for an optical galaxy at this location. However, MOST's resolution of 43 arcseconds will not resolve the core in most cases, and so other methods are necessary.

An optical galaxy near the centroid of a double source or overlapping the central region of a triple source was taken as a good optical identification. For a double source the host galaxy should lie between the lobes, near the centroid of the radio emission and along the axis defined by the linear source. In the twin beam

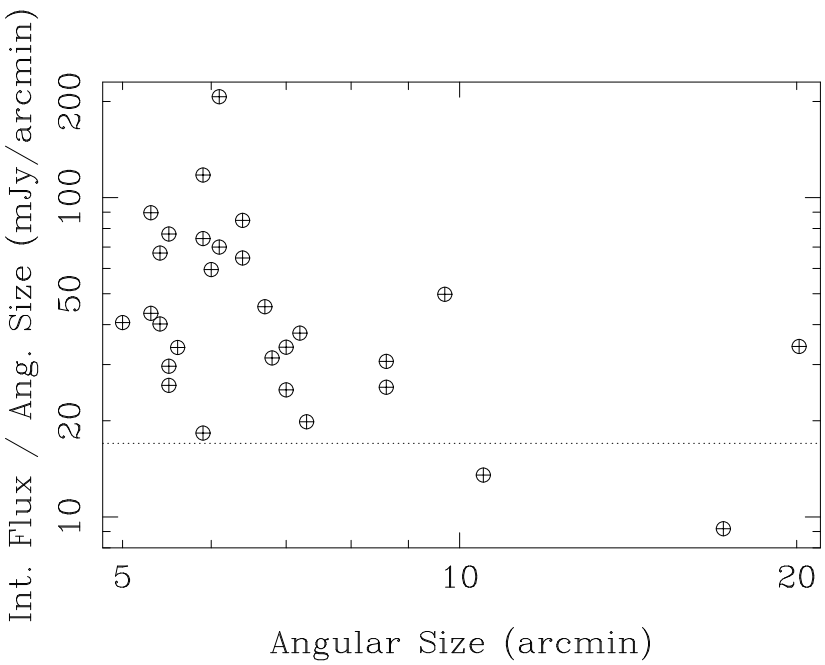

Figure 2.3: The sensitivity parameter Σ for all the giant candidates with angular sizes greater than 5 arcminutes.

model the jets leave the host galaxy with equal energy. The total energy entering each lobe should be the same, whether it spreads out or stays close to the host. For this reason the centroid of the radio emission is the best place to look for a host - this should be the origin of the radio emission. Many of the radio sources were triples, with a central region corresponding to the core and jets leaving the core at scales too small for MOST to resolve. This central region should certainly coincide with the optical counterpart.

There were some cases where it was only possible to make a tentative optical identification, with the possibility that a fainter galaxy was in fact the host. For some sources there were two plausible hosts, both close to the centroid. In other cases, there was no optical galaxy near the centroid and it was necessary to choose a galaxy some distance away. In both cases the optical counterpart was taken to be the brightest galaxy which might be the host. However, the identification was only tentative and a fainter galaxy may actually be the host. A higher resolution radio image might reveal a radio core overlapping a faint galaxy, or a more sensitive optical images might reveal a faint galaxy not seen on the DSS.

For other objects there was no optical galaxy visible near the radio source. One possibility is that the the optical host is too faint to appear on the DSS, because it is distant or obscured by dust. Another possibility is the candidate radio galaxy is not a connected structure; there is no optical host between the lobes because they are in fact two unrelated structures which happen to lie near each other in the sky.

The optical counterpart to J1919-799 was found in a different manner to the others. This source was observed in a previous survey (Subrahmanyan et al., 1996). Follow-up radio observations found a core not seen on SUMSS, and follow-up optical images located a faint galaxy coinciding with the core. See Section 5.1 for more details.

The presence of an optical counterpart boosted the case for a candidate being a genuine connected structure. A source with a giant type radio morphology and an optical host in the right location to generate the lobes is clearly a more plausible detection than a source with the giant morphology but no optical counterpart. The lack of an optical counterpart suggests either that the host galaxy is faint (and therefore distant) or that the two lobes are one source but a chance alignment of two unrelated sources.

Of the 29 candidates which exceeded 5 arcminutes in size, 15 had good optical identifications, nine had possible optical identifications and five had no plausible optical identification. Their observed radio and optical properties are listed in Appendix B.

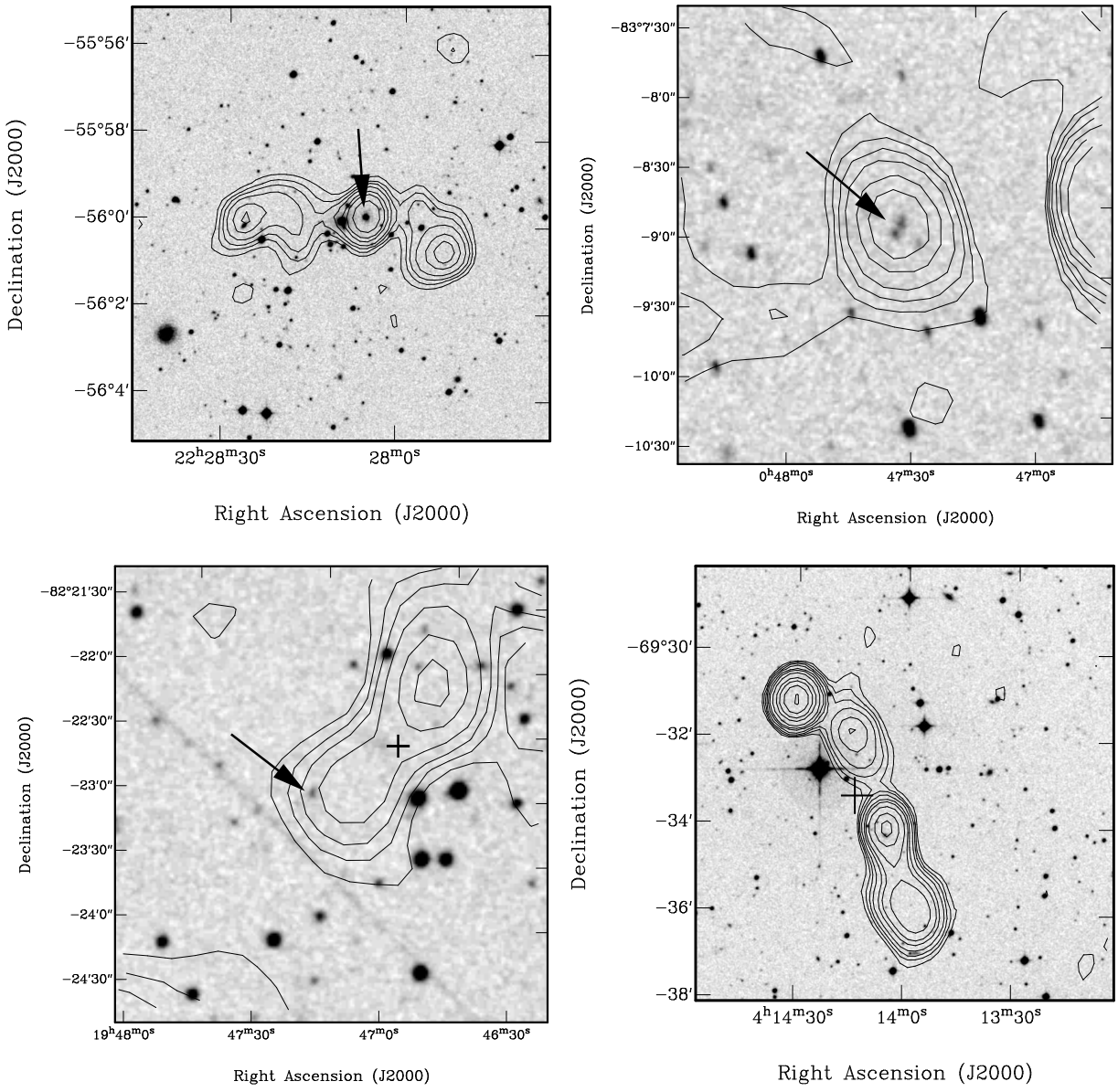

Figure 2.4: Sources with different optical identification status. All images have SUMSS contours overlaid on DSS greyscale, with good or possible optical identifications marked by an arrow. (top left) J2228-560, a good optical identification. The central region of the radio emission coincides with an optical galaxy. (top right) J0047-831, a source with two optical galaxies within the central region. Either of these could be the host. (bottom left) J1946-823, a source where the nearest optical galaxy is some distance from the centroid (marked with cross). (bottom right) J0414-695. There is no optical galaxy near the centroid (marked with a cross). The only bright objects near the centroid or the regions on the source axis near the centroid are stars. It is possible that the candidate is in fact two separate objects which happen to be aligned in the sky.

Chapter 3

Properties of the Sources

The key physical parameters are derived for the giant radio galaxy candidates.

3.1 Spectroscopic Redshifts

Accurate spectroscopic redshifts were obtained for the optical hosts of five of the candidates. One source, J1919-799, already had a redshift from previous work (see Chapter 5). Four optical identifications were made sufficiently early to allow an application for spectroscopic observations. These sources were observed as an Anglo-Australian Telescope service time observation, with integration times times between 1200s and 3600s, depending on the source brightness and observing conditions.

Reduction of the spectral data involved removing cosmic ray impacts from the data, summing the emission over the source and removing the contribution from the sky. The observed wavelengths of six well defined absorption lines were measured, and calculated the redshift z = (λ_{ob} / λ_{em}) - 1.

The spectra are plotted in Appendix B.

3.2 Estimating Redshifts

Besides the five candidates with spectroscopic redshifts there were ten sources with good optical identifications but no redshift. For these sources I estimated the redshifts using the magnitudes of the optical counterparts. The hosts of radio galaxies tend to be giant elliptical galaxies with absolute b_J magnitudes fairly constant around $M_J = -21 \pm 0.9$ (Jones, 1990). The apparent visual magnitude will then depend mostly on the redshift and hence the distance of the source.

I used a method developed by Burgess, who found that the logarithm of the redshift is proportional to the b_J magnitude (Burgess, 1998). A plot of the five counterparts for which I had spectroscopic redshifts with Burgess' (see Figure 3.1), showed that this relationship was good for these five counterparts as well. With only five sources I could not determine an accurate line from my data alone, so I decided to use the existing relationship:

$$b_J = 23.0 + 5.8log(z) \tag{3.1}$$

The redshifts were estimated in this way for the ten good optical counterparts without spectroscopic data and for the nine possible counterparts.

3.3 Physical Properties

The radio power, P, and linear size, D, can be calculated from the total radio flux, the angular size and the redshift (see Appendix D). For sources with a good optical identifications the redshift or approximate redshift was known, and so the physical properties could be calculated quite readily.

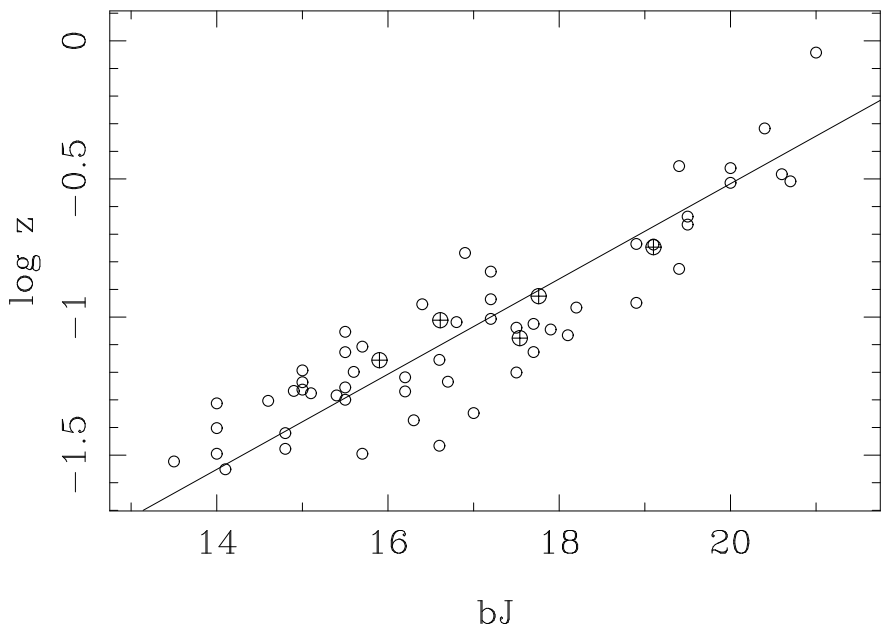

Figure 3.1: The relationship between optical magnitude and redshift, for Burgess' sources (circles) and my five sources with spectroscopic redshifts (crossed circles). The line is the fitted relationship given by Equation 3.1.

Sources without definite optical identifications posed a problem, since they did not have even approximate redshifts. These sources have been plotted as lines on the P-D diagram. Each point on the line corresponds to a particular redshift, and so the source must lie somewhere on this line. The lines are plotted only between 843 MHz radio powers of $10^{24.6}$ and 10^{27} W/Hz, since giant sources generally have powers in this range (see Schoenmakers, 1999 and Ishwara-Chandra & Saikia, 1999). The possible identifications are shown as circles on these lines. If the assignment of the counterparts is accurate, then this is the appropriate value for the source. If it is incorrect, then the actual counterpart will be fainter and more distant, so the source will have a greater linear size and redshift, and be farther along the line towards the top and right.

The resultant plot of power versus linear size is shown as Figure 3.2. This plot, known as a P-D diagram, is central to radio astronomy, as it summarises the most important physical properties of the sources. There are a few sources which have linear sizes less than 1 Mpc, but the majority of candidates are classified as giants, with sizes greater than 1 Mpc.

There are no sources at the lower right of the diagram as a consequence of the sensitivity limit. Large, faint objects will have such low flux density in their lobes that the signal will be dominated by noise and the lobes will not be observed. Radio power is proportional to integrated flux density, while linear size is proportional to angular size (see Appendix D), meaning that the sensitivity paramater Σ defined in Section 2.3 is proportional to radio power divided by linear size. Its minimum value defines a region in which a source will not be observed in this survey. The exact boundary of the region depends on the redshift of the source - the dashed lines in Figure 3.2 are upper bounds to the excluded region for two representative redshifts. Note that at higher redshifts only higher powered sources can be observed - this is an example of the Malmquist bias (see Section 1.7.1).

Note that the sources without good optical identifications lie in the same region of the P-D diagram as the other sources, and so they should not greatly affect conclusions drawn about the survey. The sources with possible identifications tend to be at the high power end of this region at, reflecting their tendency to be at high redshifts, where the optical hosts are farther away and fainter (see Section 2.4).

3.3.1 Status of J0745-775

The source J0745-775, which generates the line at the lower right of the P-D diagram, has very different properties to all other sources. For typical giant powers the linear size is at least 3 Mpc. Moreover it is well below the sensitivity limit (defined in terms of Σ) unless it is at very low redshift, in which case the absence of an optical host is puzzling. This lack of an optical counterpart or violation of the sensitivity limit casts doubt

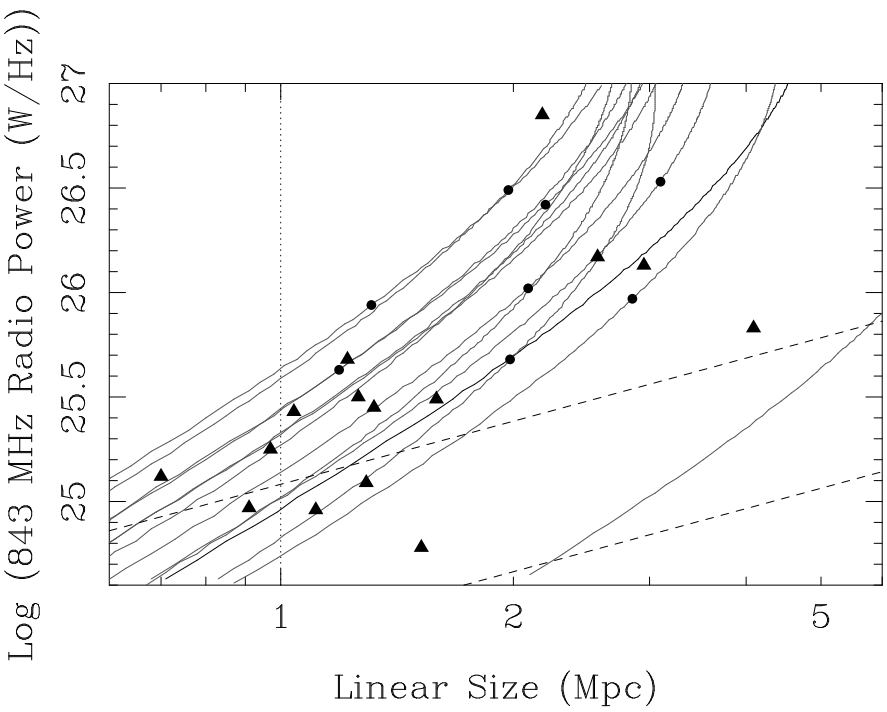

Figure 3.2: P-D diagram for the GRG candidates, assuming Ω_m = 1.0, Ω_Λ = 0 and H_0 = 50 $kms^{-1}Mpc^{-1}$. Triangles are the fifteen sources with good optical identifications, circles are the nine sources with possible optical identifications. The solid lines trace out possible values for the fourteen candidates without good identifications (this includes the possible optical identifications). The dashed lines are sensitivity limits for redshifts of 0.05 (lower line) and 0.20 (upper line). At the given redshift, sources must lie above these lines due to the limited sensitivity of SUMSS.

on whether this is a genuine source. A radio image shows six sources in a row (see Figure 3.3). Some sources are slightly extended towards each other but there is no observable connection between them. Since there is no connected structure and the physical properties are extreme, it is quite likely that this candidate is not a connected structure but a chance alignment of unrelated single or double sources.

3.4 Number of Sources

This survey found 29 candidate giant radio galaxy candidates (Section 2.2.2). If we consider only those sources with good optical identifications and linear sizes in excess of 1 Mpc then there are twelve giant radio galaxies in the sample, and three radio galaxies with sizes less than 1 Mpc. Note that many of these linear sizes are approximate since they rely on redshifts which were only estimated from optical magnitudes, so the sources with calculated sizes less than 1 Mpc may still be considered candidate giant radio galaxies. In addition there are fourteen other sources for which the optical identification is tentative or non-existent, and these sources are still candidates.

The area of sky surveyed was ∼2100 square degrees (see Section 2.1.1). Hence the density of definite giant sources is ∼ 1 per 175 square degrees. The space density of giants plus candidate giants is ∼ 1 per 70 square degrees.

The other large, uniform survey of giant radio galaxies was that of Schoenmakers (1999). This space density of giants in this survey was ∼ 1 per 165 square degrees. Schoenmakers was able to obtain spectroscopic and high resolution optical data for most of his sources, and so this detection rate is better defined; candidates were either confirmed or rejected as GRGs. With the appropriate follow-up observations my detection rate should be between the two limits from the previous paragraph, which would be roughly consistent with Schoenmakers.

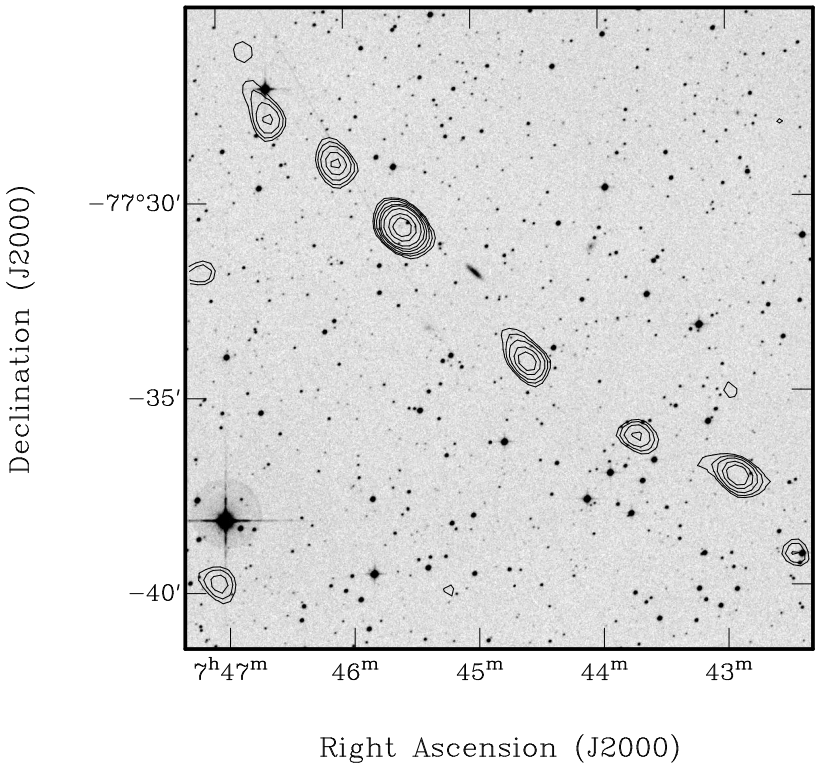

Figure 3.3: The unusual candidate J0745-775. Is this one connected structure or a chance alignment?

3.5 The Effect of Cosmology

The calculation of the physical parameters is dependent on cosmological parameters. Varying these parameters changes the formulae for calculating linear size and radio power from the observational data. Until recently the uncertainties in the cosmological parameters were very large and different techniques returned different results. With such uncertain experimental data the choice of model universe was largely arbitrary. As mentioned in Section 1.2, most previous giant radio galaxy work has assumed an Einstein - de Sitter universe (matter density $\Omega_m = 1$, cosmological constant $\Omega_\Lambda = 0$) and a Hubble constant H_0 = 50 kms^{-1}Mpc^{-1}.

However, recent measurements using a range of techniques are converging on values $\Omega_m \sim 0.3$, $\Omega_\Lambda \sim 0.7$ and $H_0 \sim 70$ kms^{-1}Mpc^{-1}. I thought it would be reasonable to compare the standard GRG cosmology with this current best estimate cosmology (see Figure 3.4). The formulae used in these calculations may be found in Appendix D.

It can be seen that the new measurements reduce both the power and size of all sources, but the relative values between sources are not greatly affected. Most of the giant candidates have z ≤ 0.4. At these low redshifts the values of Ω_m and Ω_Λ make little difference to the physical properties, and changes in size and power^2 are linearly proportional to changes in H_0. The different cosmologies move the sources around in a linear fashion on a logarithmic P-D diagram. Any conclusions drawn under either cosmology are valid in the other, except for a rougly constant shift in the P-D diagram.

Note that assuming H_0 = 70 kms^{-1}Mpc^{-1} means that many sources now classified as giants in fact have projected linear sizes less than 1 Mpc. This will apply not just to my sample but to many of the sources in the literature. Since the giants are the extreme tail of the radio galaxy distribution, the lower size limit is largely arbitrary, and it would not matter too much if some sources near 1 Mpc were reclassified, or if the size limit were changed to include all current giant radio galaxies.

Conclusions about my sample made using the standard cosmology will still be valid under the new cosmology. Thus there is no problem with using the Einstein-de Sitter universe, and this assumption makes it easier to compare my results with those of previous studies. For the rest of this thesis I will assume Ω_m = 1.0, Ω_Λ = 0 and H_0 = 50 kms^{-1}Mpc^{-1}.

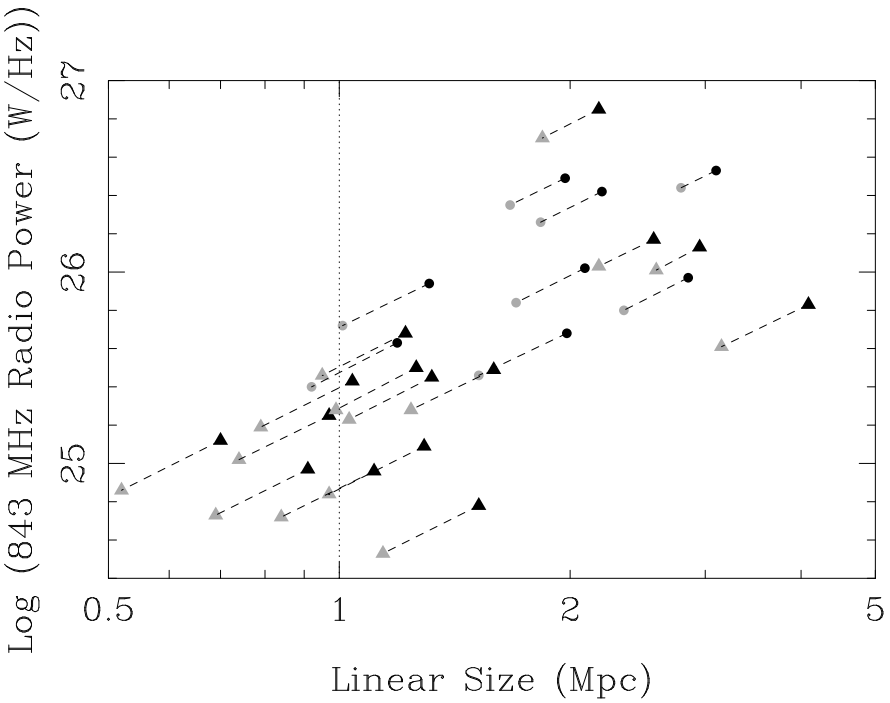

Figure 3.4: Physical properties of the GRG candidates for the standard literature cosmology, Ω_m = 1.0, Ω_Λ = 0 and H_0 = 50 kms^{-1}Mpc^{-1} (black figures) and the current best estimate cosmology, Ω_m = 0.3, Ω_Λ = 0.7 and H_0 = 70 kms^{-1}Mpc^{-1} (grey figures). The two values for each source are linked. Triangles are sources with good optical identifications, circles are sources with uncertain optical identifications. Note that for these low redshift objects most of the variation is due to the change in H_0.

Chapter 4

Discussion of the Giant Radio Galaxy Sample

The sample of giant radio galaxies is compared with previous surveys and theoretical models of radio galaxy evolution. Some interesting sources with unusual properties are identified.

4.1 Analysis of P-D Diagram

So that the sources might be compared with Schoenmakers' sample, the powers at 843 MHz were converted to 325 MHz. The spectral index (defined by $S_\nu \propto \nu^\alpha$) was assumed to be α = -0.8, which is typical for giant radio sources. The combined P-D diagram for this survey and Schoenmakers' survey is shown in Figure 4.1.

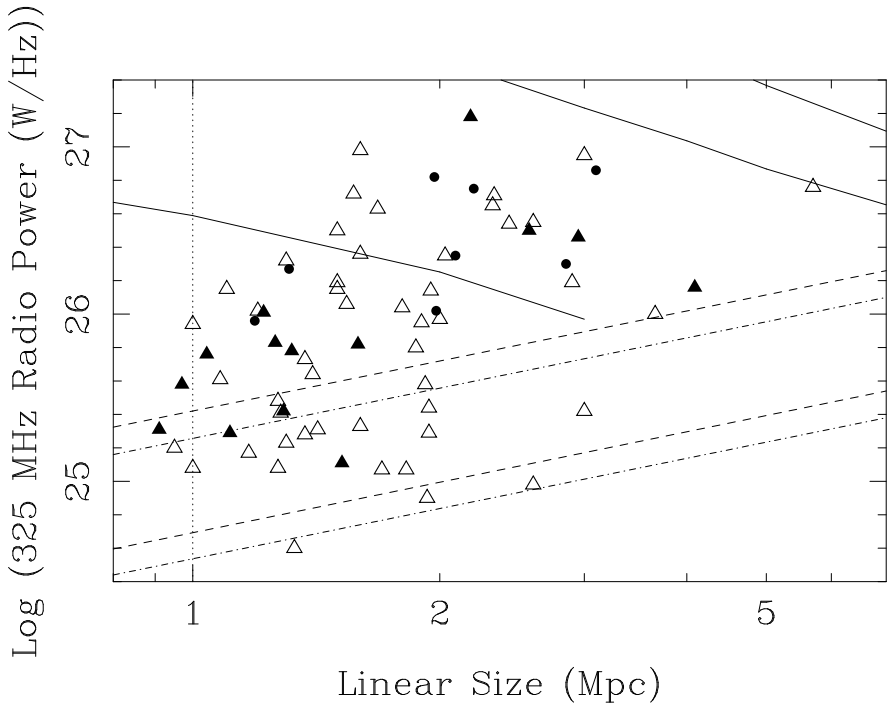

Figure 4.1: P-D diagram for my sample (filled) and Schoenmaker's sample (open) of giant radio galaxies, assuming Ω_m = 1.0, Ω_Λ = 0 and H_0 = 50 $kms^{-1}Mpc^{-1}$. Triangles are sources with good optical identifications, circles are sources with tentative optical identifications. One of my candidates at D=0.7 Mpc is omitted. Solid lines are theoretical models of radio source evolution (moving down and to the right with time) for jet powers of 1.3×10^{40}W (upper line), 1.3×10^{39}W (middle line) and 1.3×10^{38}W (lower line). Diagonal lines are sensitivity limits for my survey (dashed) and Schoenmakers' survey (dot-dash), for redshifts of 0.05 (lower pair) and 0.20 (upper pair).

It can be seen that my sources overlap well with those of Schoenmakers. This is to be expected, since we searched from similar datasets, and applied similar search criteria. Schoenmakers' sample extends a bit farther into the lower right of the P-D diagram, which reflects the lower sensitivity limit of that sample.

4.2 Consistency with Evolutionary Models

The models of radio galaxy evolution predict that as the galaxies age they spread out in space but radiate away energy, so they become larger and less powerful with time. (cf. Section 1.4). Three lines superimposed on the P-D diagram showed this predicted evolutionary path for three radio galaxies with given initial jet powers (Kaiser et al., 1997). The models suggest that there should not be any sources in the top right of the diagram, where they would be both large and powerful; and that there should be many sources in the lower right of the diagram, which is the endpoint of an expanding, de-energising galaxy.

There is indeed a lack of large, high power sources, as predicted. If present, such sources should be easy to observe; their absence bolsters the theoretical models. However, no sources are seen at the lower right of the diagram, due to the surface brightness limit. Objects in the lower right of the diagram are large and faint and their surface brightness is so low that their lobes cannot be distinguished from the field noise. The sensitivity limits (see Sections 2.3 & 3.3) are closely related to surface brightness and exclude sources in the lower right region from the surveys. To find such large low power sources it would be necessary to have a better surface brightness sensitivity, achieved by increasing the collecting area or the integration time. When the SUMSS mosaics are complete the surface brightness limit might be lowered and sources might be found to populate part of this region of the P-D diagram.

4.3 J0331-771

Analysis of the P-D diagram reveals one source with the very large projected linear size of 4.1 Mpc. Such a size would make this the second largest giant radio galaxy in the literature (the largest, 3C236, appears in the Schoenmakers sample). Such an unusual source prompts questions. Is the source really one connected structure? Have we made the correct optical identification? Is the redshift accurate?

To test the status of this galaxy, observations were made using the Australia Telescope Compact Array. Various radio contours overlaid on optical greyscales are shown in Figure 4.2.

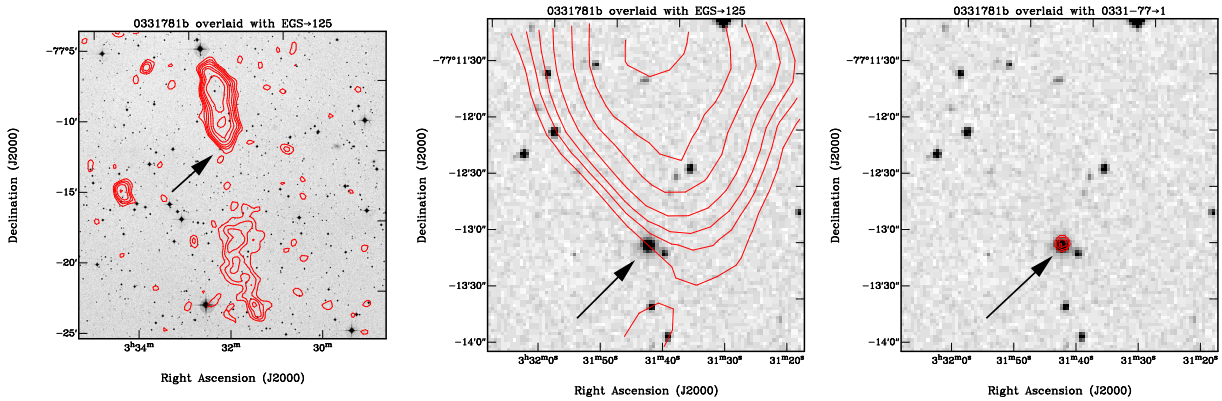

Figure 4.2: The giant radio galaxy J0331-771. The arrow indicates the optical host in all three plots. (left) SUMSS 843 MHz contours on Digitised Sky Survey (DSS) greyscale. Contours at 3, 5, 7, 10, 15, 20, 30 mJy/beam. (middle) The same, magnification of the region near the host. (right) Australia Telescope 1.4 GHz contours on DSS greyscale. Contours at 0.5, 0.7, 1, 1.2 mJy/beam. A compact radio source, assumed to be the core, coincides with the optical host galaxy.

A compact radio source was observed only between the lobes and not within either lobe. If we take this source to be the core then J0331-771 is one connected structure and not two unrelated objects. Since the compact source overlies the optical galaxy, we may be quite confident of this identification.

The remaining uncertainty concerns the redshift of the host galaxy. This was only an estimate, based on the host's optical magnitude of b_J = 18.20 (see Section 3.2). Examination of Figure 3.1 suggests that the redshift could be in error by 0.05 at this optical magnitude. Hence the projected linear size might as low as 3.0 Mpc.

The source is indeed a single giant radio galaxy. Its classification as the second largest radio galaxy known must be tentative until optical spectroscopic data is available. If the 4 Mpc linear size is confirmed then the source fills a gap in the P-D diagram between the giants with linear sizes $\leq$ 3 Mpc and 3C236 at 5.7 Mpc.

4.4 Double-Double Sources

Double-double source are those in which there are multiple pairs on either side of the host galaxy, with corresponding hotspots at similar distances from the centre and having similar morphologies. There were six sources in this sample with a double-double morphology, shown in Figure 4.4.

The significance of these objects was explained in Section 1.6. Such sources are thought to be the result of the jets from the AGN stopping and restarting after some time. The new jet enters the lobe of the old and starts a new hotspot. This may occur within the lobe, although this is difficult as the lobe is much less dense than the intergalactic medium (IGM). Alternatively the new jet may be aligned in a different direction and so it may encounter the IGM outside the old lobes, forming new smaller lobes.

It is worth noting that in five of the six double-double sources the outer pair of hotspots is more spread out and diffuse than the inner pair (J0331-771 being the only exception). This is consistent with the model described above. The old hotspot is the location of the shock front formed by the old jet. However, this jet has not been active for some time and so the energised particles have had time to spread out, forming a more diffuse region. The new hotspot has an active jet powering it at the time of emission and so there is a compact centre of emission at this new hotspot.

For two of the double-double galaxies (J2159-723 and J2336-818) the axis defined by the inner hotspots is slightly skewed from that defined by the outer two hotspots. The jets have shifted to a different axis between the two episodes of jet formation. One possibility is that between episodes of jet activity the orientation of the black hole accretion disk precesses, pointing the restarted jets in a new direction. Another possibility is that the immediate environment of the active galactic nucleus changes between the two jet formation episodes and the changed environment bends the jets in a different direction.

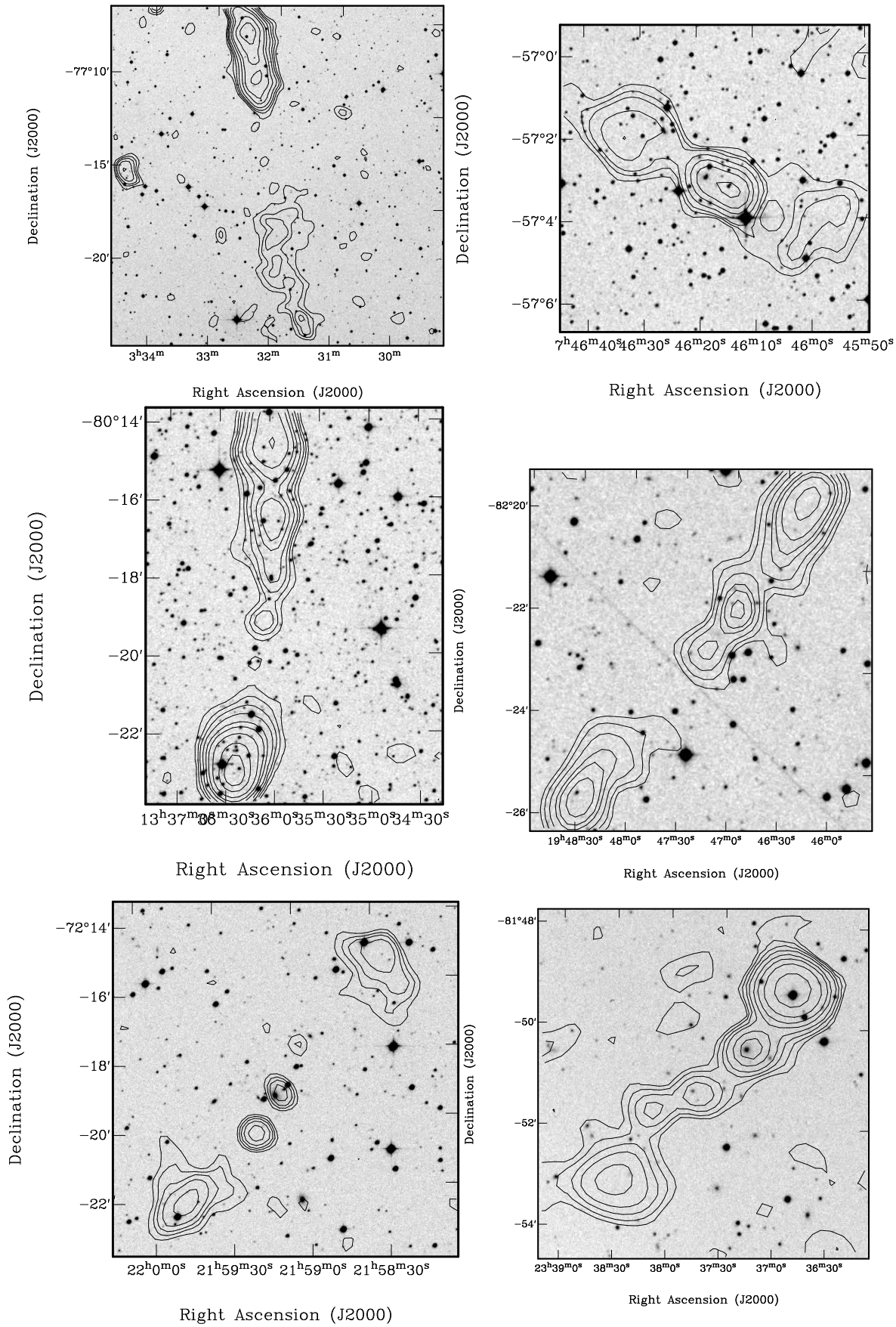

Figure 4.3: Six candidate giant radio galaxies with a double-double morphology. (top left)J0331-771. (top right)J0746-570. (middle left)J1336-803. (middle right)J1946-823. (bottom left)J2159-723. (bottom right)J2336-818.

Chapter 5

Detailed Study of J1919-799

A detailed study of one giant radio galaxy, J1919-799, has been made using high resolution, multi-frequency images from the Australia Telescope Compact Array.

5.1 History of J1919-799

J1919-799 is as the most powerful object in my sample. It is hardly surprising that this source, also known as B1910-800 after its B1950.0 co-ordinates, was part of an earlier sample of powerful megaparsec sized radio galaxies (Subrahmanyan et al., 1996). The eight members of this sample were drawn from an earlier MOST survey of extended sources (Jones & McAdam, 1992), and were imaged at high resolution at a frequency of 1.4 GHz using the Australia Telescope Compact Array (ATCA).

Jones & McAdam had made an optical identification using only SUMSS and the Digitised Sky Survey (DSS). The high resolution ATCA image revealed a core which did not coincide with their tentative optical identification, or indeed with any other optical galaxy visible on the blue-sensitive DSS.

Inspection of the original plates from which the DSS was scanned revealed that there was considerable obscuration of the optical field by gas and dust from within our galaxy. This material made the optical host too dim to be seen on the DSS or the original blue survey plate. The red survey plate showed a faint galaxy coincident with the radio core; galactic dust had extinguished it in the blue. After locating the host, a deeper image and a spectrum were obtained at the Anglo-Australian Telescope, and the redshift was found to be z = 0.346.

5.2 Imaging with the Australia Telescope

The observations for the original Subrahmanyan et al. survey were made at a frequency of 1.4 GHz with three different array configurations. Follow up observations were made at three frequencies: 1.4 GHz, 2.4 GHz and 5.8 GHz; and in four configurations: 375, 750C, 1.5D and 6C. There was also one observation at 8.8 GHz in the 6C configuration. The follow-ups thus included about as much information as could be expected for the source for frequencies other than 8.8 GHz.

The data reduction was done using the Miriad data reduction package. It involved flagging, calibration, imaging, deconvolving, restoring and self-calibration. A flow-chart for these procedures is shown in Figure 5.1.

The steps in the procedure were as follows:

Flagging After being loaded from the telescope the original data was contaminated by terrestrial interference. The data were examined using the `uvplt` routine and channels affected by noise were flagged using `uvflag` and `tvflag`.

Calibration The data were then calibrated. A standard unpolarised calibrator, B1934-638, whose flux is known very accurately, was used to calibrate the flux of a secondary calibrator, B1903-802, using `mfcal, gpcal and gpboot`. Observations of the secondary calibrator were used to calibrate the

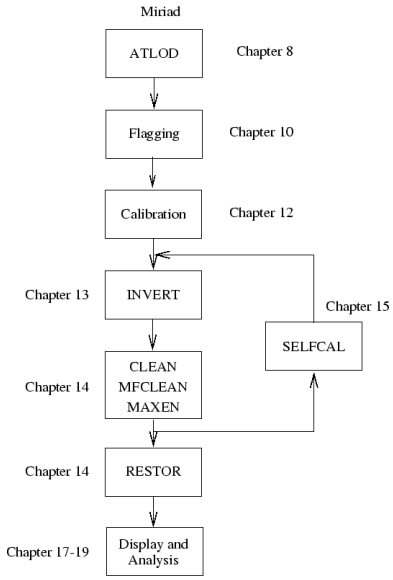

Figure 5.1: A flow chart for the Miriad imaging process (Sault & Killeen, 1999). Chapter numbers refer to chapters in the Miriad manual, from which this diagram is taken.

amplitude and phase gains of the antennae and equipment. These calibration tables were transferred to the data of the target using `gpcopy`.

Imaging Radio telescopes generate visibility data, which is a Fourier Transform of the sky signal. The visibilities were converted to a sky image using `invert`, which performs the inverse Fourier Transforms.

Deconvolving A sparse array of discrete antennae will generate strong sidelobes around any source that it images, due to diffraction effects. A raw image is contaminated by sidelobes from all the strong sources in the field. The CLEAN algorithm, implemented by the routine `clean`, was used to remove these telescope artefacts. The algorithm locates the strongest pixel, models the beam generated by a point source at this location, subtracts a fraction of this emission from the image and notes the strength of the source which has been removed from the image. This process is repeated until all sidelobes are below the noise level. It was necessary to make sure that the algorithm subtracted only a small fraction of the emission for each peak pixel, as a single bright point source was not an accurate fit to the extended structure of the galaxy.

Restoring The CLEANed residual image and the file of fitted sources was used to generate an output image using the routine `restor`. For every source subtracted by `clean`, `restor` adds a Gaussian source of the appropriate strength. The combined effect of `clean` and `restor` is to replace the telescope beam and all its artefacts with a Gaussian beam, so that the sources appear as Gaussian sources and not as telescope diffraction patterns. Extended sources, such as the giant radio galaxies, are reconstructed from hundreds or thousands of overlapping weak gaussian components.

Self-Calibration Throughout an observation the gains of the equipment are not constant. Self-calibration takes a model of the source from a CLEANed image and varies the calibration so that at any given time the visibilities vary least from the expected visibilities of the modelled source. The routine `selfcal` was used to self-calibrate the data.

After self-calibration the recalibrated data were used to repeat the imaging, deconvolving and self-calibration in a cyclic fashion. After about three rounds of self-calibration the image was not improved by further repetitions of the cycle, so the final image was restored at this point

The end products were images of J1919-799 for three frequencies - 5 GHz, 2.3 GHz and 1.4 GHz. These three images and the 843 MHz image from SUMSS are plotted as Figure 5.3.

5.3 Interpretation

The effects of spectral ageing (see Section 1.1.3) can be clearly seen. A strong nearby source generates too much noise for the changes in spectral index to be calculated accurately but there are marked changes in the lobe structure.

At 5.8 GHz there is a gap of ∼1.3 arcminutes between the core and detection of the lobes; this gap is ∼0.8 arcminutes for 2.4 GHz and only ∼0.6 arcminutes for 1.4 GHz. Regions with old plasma have lost most of their high energy electrons and emit little high frequency emission, but still have lower energy electrons emitting at lower frequencies. The fact that the central regions can only be detected at lower frequencies shows that the plasma here is old; the jets have transported new plasma from the active nucleus directly out to the edges of the lobes.

The northern lobe hotspot is much brighter than the rest of the lobe at 5.8 GHz, while the difference is less marked at 2.4 GHz and even less so at 1.4 GHz. This shows that the spectrum is flatter in the hotspot than the rest of the lobe and so the youngest, most energetic plasma has been deposited in the hotspot, not the whole lobe.

5.4 A Wandering Jet?

There is some evidence from the 5.8 GHz data for multiple hotspots in the northern lobe (see Figure 5.2) It can be seen that there are two separate peaks in this region. Such multiple hotspots suggest that the jet direction has shifted due to magnetic field and density perturbations. When the jet moves slightly the point where the jet meets the IGM shifts, and a new shock is formed.

Such details should be seen better in an 8.8 GHz observation, which has higher angular resolution. Unfortunately the 8.8 GHz data came from only a single observation and the receiver is noisy in the 8.8 GHz band. The signal to noise ratio was too low to generate a meaningful image. Further observations at 8.8 GHz would be necessary to image the multiple hotspots accurately.

There is some evidence for two hotspots in the southern lobe as well (see 5.3), although these are much further apart than their northern counterparts.

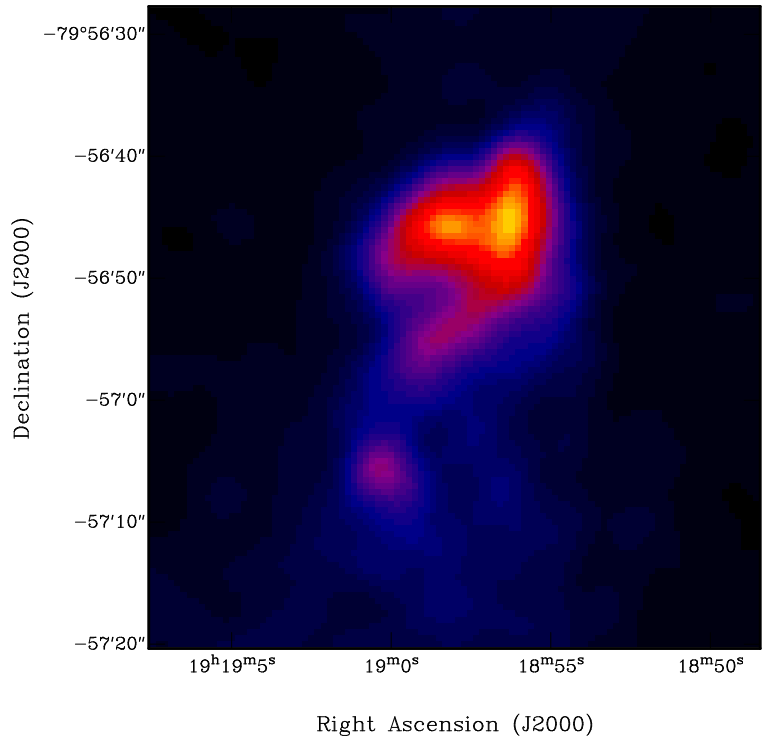

Figure 5.2: The northern hotspots and lobe of J1919-799 at 5.8 GHz.

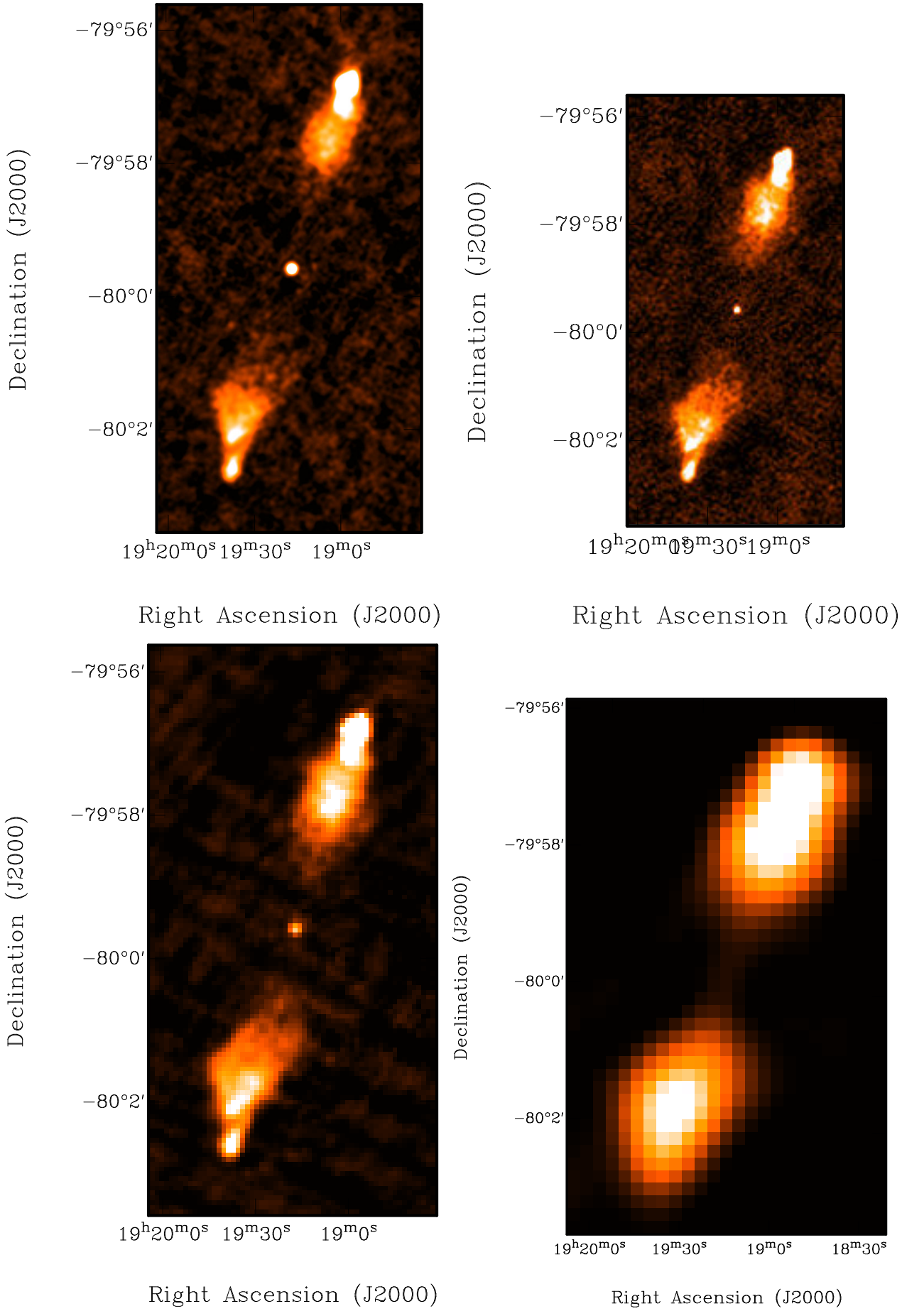

Figure 5.3: J1919-799 at 5.8 GHz (top left), 2.4 GHz (top right), 1.4 GHz (lower left) and 843 MHz (lower right). The image intensity levels and colour schemes are the same for all sources.

Chapter 6

Interlopers and Remnants

Some interesting sources were found during the search procedure besides the giants. These are discussed briefly here.

6.1 Cluster Sources

Two head-tail sources were found in the search process (see Figure 6.1). These were at first confused with GRGs because they are connected structures with angular sizes greater than five arcminutes.

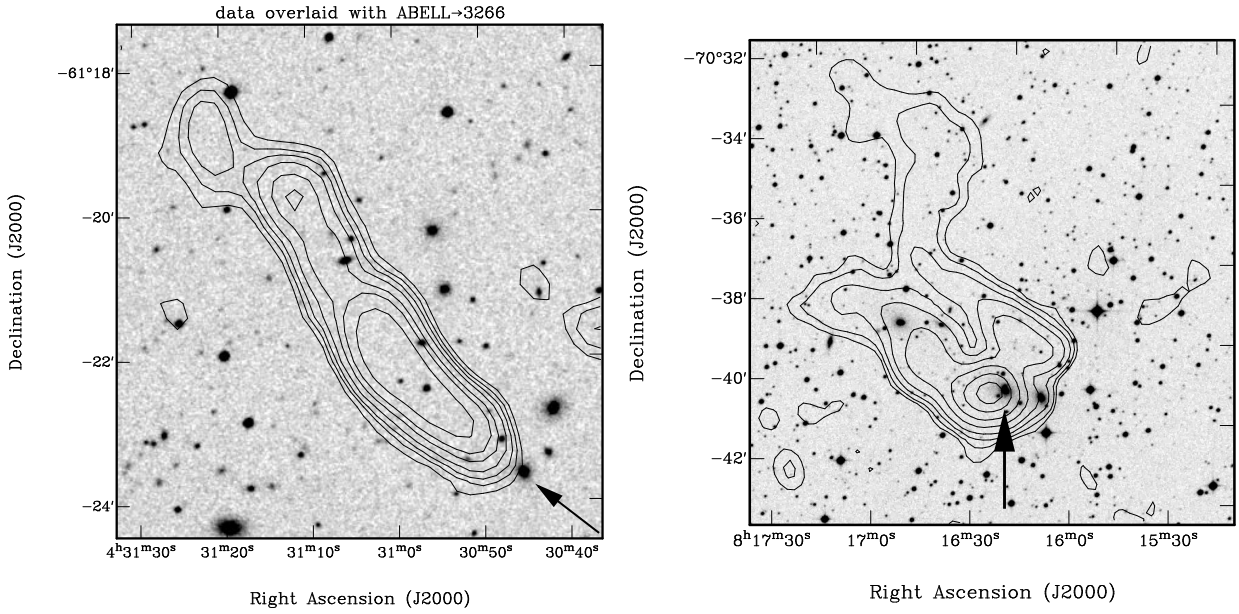

Figure 6.1: The head tail sources J0431-613 (left) and J0816-706 (right). Contours for J0431-613 are set at 3, 5, 7, 10, 15, 20, 30 mJy/beam. Contours for J0816-706 are set at 3, 7, 15, 30, 70, 150, 300, 500 mJy/beam. Arrows mark the likely optical counterparts.

Sources such as these are found in dense environments and many bright galaxies are visible in the optical fields. Galaxies move at speeds of 500 to 1000 km/s in a cluster due to gravitational interactions. An active galaxy travelling at this speed through a dense intracluster medium will leave old plasma trailing behind it (the tail of the source) and generate new plasma at the present location of the galaxy (the head of the source).

Since these sources form in a quite different environment to the giants, they have different properties and it is beyond the scope of this project to analyse the sources in any depth. J0431-613 is discussed in another work on cluster sources (Murphy, 1999), while J0816-706 is part of a survey on general extended sources (Jones & McAdam, 1992). However, it is worth noting that SUMSS has detected additional diffuse emission in the northern lobe of J0816-707, which was not observed in the earlier MOST image.

6.2 One Lobe Sources - Faded Remnants?

As mentioned in Section 1.4 giant radio sources spread out and fade as they age. Eventually they become so diffuse that they are below the surface brightness limit of telescopes such as MOST. In many radio galaxies the lobes are asymmetric (a good example is J0331-771, see Section 4.3). One lobe seems to have faded more than the other, perhaps due to differences in the intergalactic medium on different sides, or different collimations of the jets from the immediate galactic environment. As the lobes continue to fade, one might expect that one lobe would become invisible while the other would still be observable.

Two such one lobe candidates have been found. It is instructive to compare these sources with double-lobed sources in which the lobes are large and diffuse (see Figure 6.2). If the fainter lobe of one of the double sources was to fade from view, the remaining lobe would resemble the one lobe sources. This suggests the one lobe sources may have originally been double sources.

The single diffuse lobes may be an endpoint of galactic evolution, when one lobe has such low surface brightness that it cannot be observed. Such single lobes will frequently be less than 5 arcminutes across and so my survey method is not suited to finding such objects. Nevertheless, they are an interesting class of object with possible connections to the giant sources and radio source evolution in general.

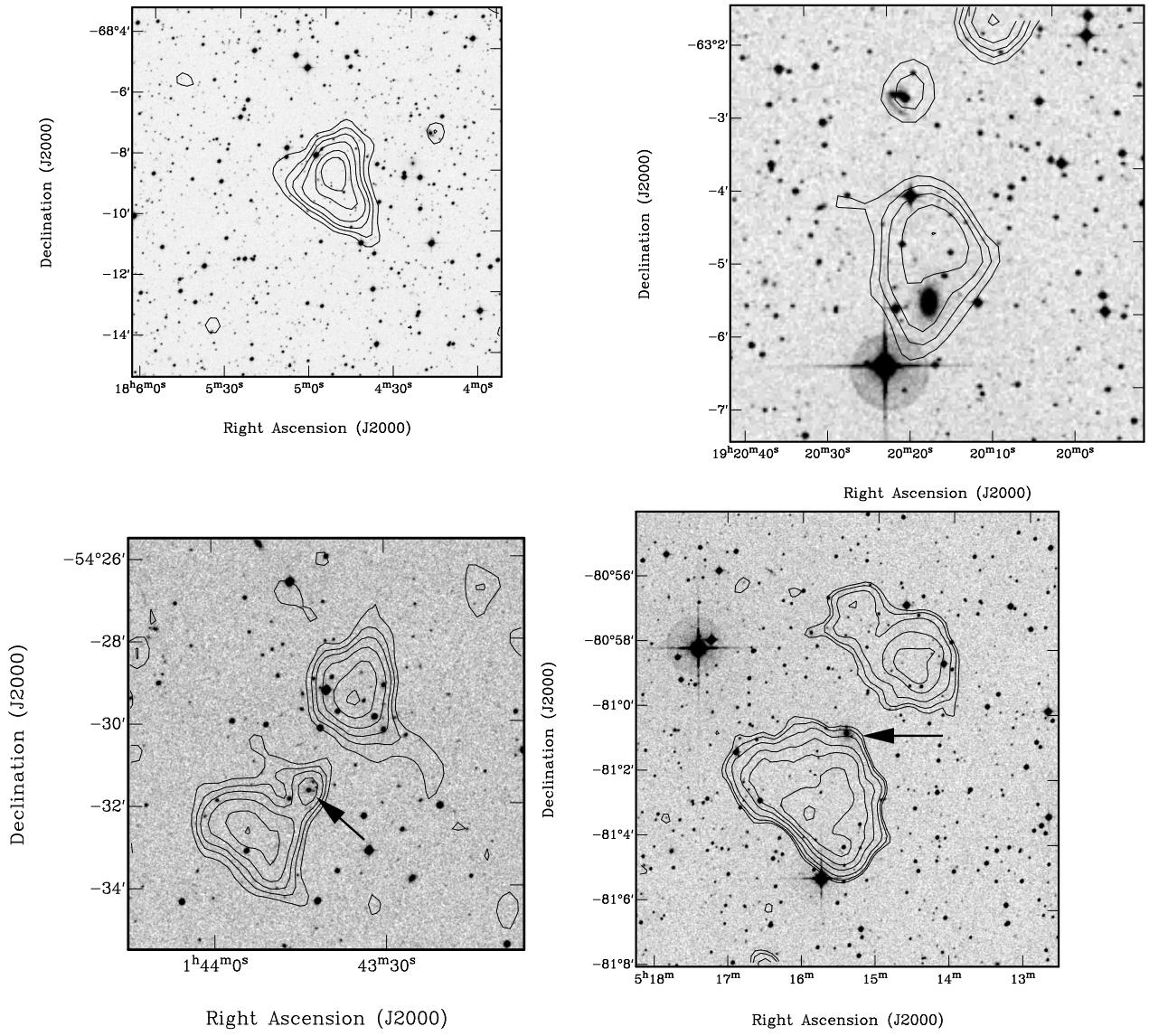

Figure 6.2: Two one-lobe sources J1804-681 and J1920-631 with two giant candidates, J0143-545 and J0515-810. Contours for J1804-681, J1920-631 and J0143-545 are set at 3, 5, 7, 10, 15, 20, 30 mJy/beam. Contours for J0515-810 are set at 1.5, 2, 3, 5, 7, 10, 15 mJy/beam. Arrows mark the optical counterparts.

Chapter 7

Conclusions

A survey of giant radio galaxies was made by scanning a subset of the Sydney University Molonglo Sky Survey (SUMSS) covering ∼26% of the final SUMSS survey area and ∼5% of the whole sky. The properties of this sample were calculated and found to be consistent with previous samples and existing models of radio galaxy evolution, although these models were not tested in great depth. Some noteworthy radio galaxies were investigated more thoroughly, which revealed the processes at work in giant sources.

7.1 Properties of the Sample as a Whole

This survey has found twelve giant radio galaxies and fourteen candidate giant radio galaxies. This corresponds to a detection rate of $\sim$ 1 per 175 square degrees for giants and $\sim$ 1 per 70 square degrees for giants and candidate giants. The characteristics of the sample do not change significantly if a different cosmology is adopted.

The properties of both the giants and candidate giants were similar to the northern hemisphere survey of Schoenmakers and consistent with theoretical models of GRG formation. The sources evolve towards lower power and larger size as they age, so there are no sources in the upper right of the P-D diagram (large sizes and high powers). The observational sensitivity limit means that no sources are seen in the lower right of the P-D diagram, at large sizes and low powers. The models predict that these unobserved sources are the final stage of a radio galaxy's evolution.

7.2 Interesting Sources

J0331-771 is apparently a 4 Mpc source straddling the gap between the dropoff in numbers at 3 Mpc and 3C236 at 5.7 Mpc.

Six double-double galaxies were found. Their morphologies demonstrated phenomena associated with restarted nuclear activity, including changes in the jet direction and a more compact morphology for the inner lobes.

The source J1919-799 was studied in detail and demonstrates several aspects of the jet theory. Spectral ageing arguments showed that the plasma in the outer region of the lobes was younger than plasma in the centre, which is consistent with the jet theory of FRII radio sources. The northern lobe showed two hotspots, suggesting that the jet direction had changed slightly.

Some faint objects that appeared to be single isolated lobes of a double lobed radio galaxy were found. These sources may be the de-energised relics of old radio galaxies.

7.3 Future Work

One future avenue is to detect more giant sources in SUMSS. This survey used only ∼26% of the survey and ∼5% of the sky; much more will become available as SUMSS is completed. As fields are combined into mosaics the noise will be reduced and radio galaxies with lower surface brightnesses will be observed. Both

developments mean that a similar survey in a few years time should find many more giant sources. With a lower surface brightness limit the lower right corner of the P-D diagram might even be filled in.

Another option for advancing the study is follow-up observations of the giants and candidate giants. High resolution radio images should detect the radio cores and allow definite optical identifications to be made. One such observation has already been made for 0515-801 (Richard Hunstead, private communication). Deep optical images might be useful to find faint optical counterparts and to explore in detail the environments which foster giant sources. Most importantly, spectroscopic redshifts for all the host galaxies would allow the physical parameters to be calculated accurately.

The high resolution images for the giant radio galaxy J1919-799 could be further improved by flagging data associated with a nearby unrelated strong source. This might reduce the noise to the point where accurate spectral indices could be calculated at all points in the lobes, with the spectral ageing revealing the history of the source in detail. More 8.8 GHz observations could show the hotspot structure in the northern lobe in more detail.

Similar detailed studies could be carried out for other giant sources. In particular, it would be interesting to see how the spectral index varies in a double-double. We might expect a flatter spectrum in the new inner hotspots, and a steeper spectrum in the old outer hotspots, in contrast to the usual distribution.

Chapter 8

Bibliography

Blundell, K.M., Rawlings, S., & Willott, C.J.:1999, *astro-ph/9907418*.

Bock, D. C.-J., Large, M.I., & Sadler, E.M.:1999, *Astron. J.*, **117**, 1578-1593.

Burgess, A.:1998, *The Molonglo Southern 4 Jy Sample: the Brightest Radio Sources in the Southern Sky*, Ph.D. Thesis (Univ. of Sydney).

De Young, D.S.:1976, *Ann. Rev. of Astron. & Astrop.*, **14**, 447-473.

Fanaroff, B.L. & Riley, J.M.:1974, *Mon. Not. R. Astron. Soc.*, **167**, 31-35.

Freedman, W.: 1999, *astro-ph/9909076*.

Fukuyita, M.: 2000, *astro-ph/0005069*.

Ishwara-Chandra, C.H. & Saikia, D.J.: 1999, *Mon. Not. R. Astron. Soc.*, **309**, 100-112.

Ishwara-Chandra, C.H. & Saikia, D.J.: 1999a, *astro-ph/9909098*

Jones, P.A.: 1990, *Proc. Astron. Soc. Aust.*, **8**, 254-256.

Jones, P.A. & McAdam, W.B.: 1992, *Astrophys. J. Supp.*, **80**, 137-203.

Kaiser, C.R. & Alexander, P.:1997, *Mon. Not. R. Astron. Soc.*, **286**, 215-222.

Kaiser, C.R., Dennett-Thorpe, J. & Alexander, P.: 1997, */astrop-ph 9710104*.

Komissarov, S.S., & Gubanov, A.G.: 1994, *Astron. Astrophys.*, **285**, 27-43.

Laing, R.A., & Bridle, A.H.: 1987, *Mon. Not. R. Astron. Soc.*, **228**, 557-571.

Lara, L., Giovannini G., Cotton W. D., Feretti L., Marcaide J. M., Marquez I., Taylor G. B., Venturi T.:1999, *astrop-ph/9909201*.

Leahy, J.P.: 1996, *Vistas Astron.*, **40**, 173-177.

Leahy, J.P., Bridle, A.H. & Strom, R.G.: 1999, *3CRR Atlas: Home Page*, http://www.jb.man.ac.uk/atlas/

Lineweaver, C.H.: 1999, *Science*, **284**, 1503-1507.

Mack, K.H., Klein, U., O'Dea, C.P., Willis, A.G., & Saripalli, L.:1998, *Astron. Astrophys.*, **329**, 431-442.

McVittie, G.C.: 1965, *General Relativity and Cosmology, 2nd ed.*, Chapman & Hall, London.

Murphy, T.: 1999, *Diffuse Radio Sources in Clusters of Galaxies*, Hons. Thesis (Univ. of Sydney).

Robertson, J.G.: 1991, *Aust. J. Phys.*, **44**, 729-42.

Sault, R. & Killeen, N.:1999, *Miriad Users Guide*, http://www.atnf.csiro.au/computing/software/miriad/userhtml.html

Schoenmakers, A.: 1999, *A Population Study of Giant Radio Galaxies*, Ph.D. Thesis (Univ. of Utrecht).

Subrahmanyan, R. & Saripalli: 1993, *Mon. Not. R. Astron. Soc.*, **260**, 908-914.

Subrahmanyan, R., Saripalli, L. & Hunstead, R.W.: 1996, *Mon. Not. R. Astron. Soc.*, **279**, 257-274.

Turner, M.S.: 1999, *astro-ph/9904049*.

Valtonen, M.J. & Heinämäki, P.: 2000, *Astrophys. J.*, **530**, 107-123.

van der Bergh, S.:1999, astrop-ph/9908050.

Witt, H.J., Mao, S. & Keetou, C.R.: 2000, *astro-ph/0004069*.

Wright, E.L.: 2000, *Astronomy 275 Lecture Notes*, University of California, Los Angeles, http://www.astro.ucla.edu/~wright/cosmolog.htm

Yentis, D.J., Cruddace, R.G., Gursky, H., Stuart, B.V., Wallin, J.F., MacGillivray, H.T., and Collins, C.A.: 1992, *The Cosmos/UKST Catalog of the Southern Sky*, in Digitised Optical Sky Surveys (editors H.T. MacGillivray and E.B. Thomson), Kluwer Academic Publishers, Dordrecht.

Appendix A

Acronyms and Symbols

α : spectral index, defined by $S_\nu \propto \nu^\alpha$, and also...
α : right ascension
ACTA: Australia Telescope Compact Array
AGN: active galactic nucleus
APM: an optical sky catalog (incomplete)
b_J: an particular blue wavelength optical magnitude which measures the response of the film used in preparing the DSS
COSMOS: an optical sky catalog
δ: declination
D: projected linear size of a radio source
DDRG: double-double radio galaxy
DSS: Digitised Sky Survey
FRI: Fanaroff-Riley Class 1 (edge-darkened) radio galaxy
FRII: Fanaroff-Riley Class 2 (edge-brightened) radio galaxy
GRG: giant radio galaxy
H_0: Hubble constant, measured in $\text{kms}^{-1}\text{Mpc}^{-1}$
IGM: intergalactic medium
kpc: kiloparsec
MOST: Molonglo Observatory Synthesis Telescope
Mpc: megaparsec
Myr: megayear
ν : frequency of radio observation
NED: Nasa Extragalactic Database
P: radio power emitted by a source
P-D diagram: plot of radio power vs. projected linear size for a population of radio sources
pc: parsec = $3.086 \times 10^{16} m$
q_0: cosmological deceleration parameter (governs curvature of universe)
S : radio flux density
S_{int} : radio flux density integrated over a whole source
SUMSS: Sydney University Molonglo Sky Survey
SuperCOSMOS: an optical sky catalog
θ: angular size of a radio source
VLA: Very Large Array
WENSS: Westerbork Northern Sky Survey
z: redshift

Appendix B

Source Data

The spectra of the four galaxies observed in the AAT service time observation are shown below.

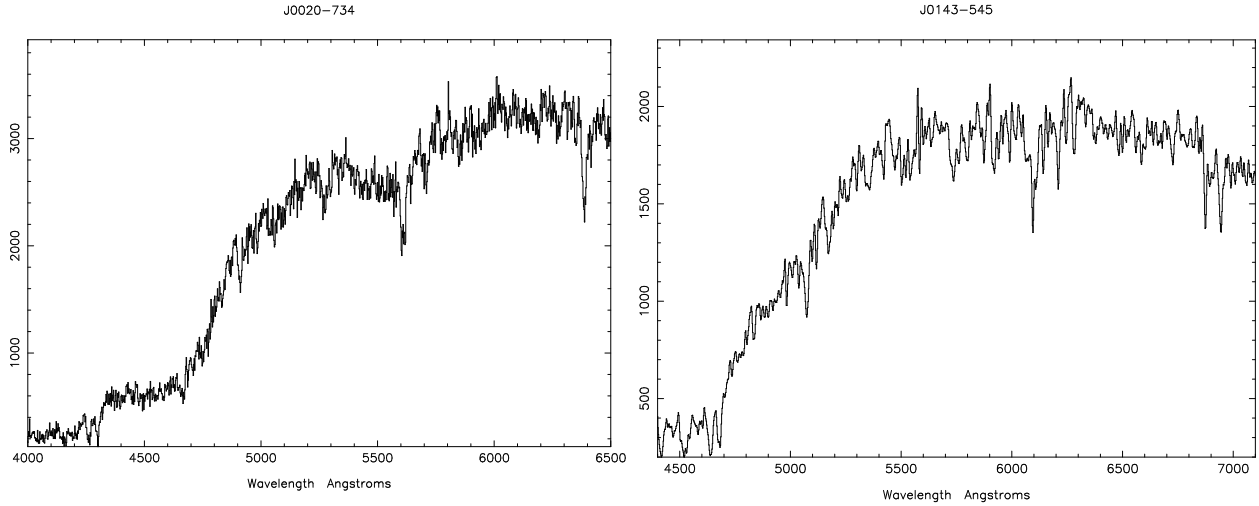

Figure B.1: (left) J0020-733, z = 0.0839±0.0001 (right) J0143-545, z = 0.1791±0.0001

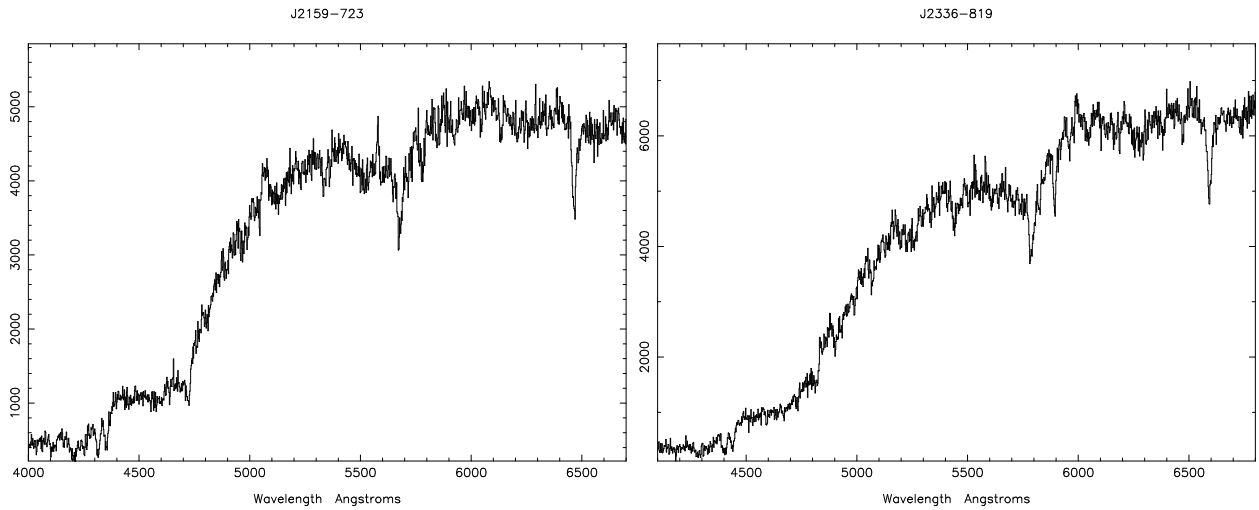

Figure B.2: (left) J2159-723, z = 0.0974±0.0001 (right)J2336-818, z = 0.1190±0.0001

Table B.1: Measured Radio and Optical Properties of All Candidates

Source name	Centroid Position α (J2000) δ	Peak S_{843} (mJy/beam)	Int. S_{843} (mJy)	θ (arcmin.)	Status	Optical Mag. b_J	b (deg.)
J0020-733	00 20 38.4 −73 21 30.2	81.6	423	5.5	good	17.54	−43.59
J0047-831	00 47 06.6 −83 07 29.5	270.6	543	6.4	tentative	20.14	−34.00
J0129-645	01 29 29.9 −64 33 41.7	70.9	362	5.4	good	18.56	−52.07
J0143-545	01 43 44.2 −54 31 04.5	21.1	217	5.4	good	19.10	−60.99
J0152-803	01 52 49.8 −80 20 25.0	167.7	305	6.7	tentative	19.73	−36.41
J0200-601	02 00 24.7 −60 07 23.5	95.5	207	4.1†	tentative	21.50	−54.96
J0237-644	02 37 08.0 −64 29 46.9	57.3	145	7.3	good	20.94	−49.00
J0326-775	03 26 16.9 −77 30 42.2	113.2	357	6.0	none	–	−36.54
J0331-771	03 31 34.6 −77 10 43.1	50.1	687	20.1	good	18.20	−36.57
J0400-849	04 00 45.9 −84 56 54.5	21.2	175	7.0	good	17.41	−30.49
J0414-695	04 14 14.5 −69 33 17.9	158.7	414	6.4	none	–	−38.62
J0515-810	05 15 56.1 −81 00 56.2	17.6	264	8.6	good	17.25	−30.44
J0534-821	05 34 25.1 −82 03 53.2	379.1	977	4.9†	none	–	−29.48
J0551-569	05 51 35.4 −56 55 27.7	676.3	864	4.3†	none	–	−30.50
J0603-544	06 03 46.2 −54 29 25.2	143.5	165	4.9†	none	–	−28.55
J0622-596	06 22 40.9 −59 38 02.3	117.6	142	5.5	none	–	−26.73
J0631-540	06 31 57.1 −54 05 13.8	191.7	694	5.9	tentative	18.48	−24.43
J0745-775	07 45 07.2 −77 32 04.0	94.6	158	17.2	none	–	−23.62
J0746-570	07 46 21.2 −57 02 45.5	55.9	194	3.3†	tentative	18.18	−15.53
J0810-680	08 10 49.1 −68 00 07.6	74.9	271	7.2	tentative	21.30	−18.04
J0843-701	08 43 13.4 −70 07 14.4	30.0	203	5.0	good	18.05	−16.68
J1259-776	12 59 11.6 −77 37 05.0	108.5	439	5.9	tentative	18.17	−14.75
J1336-803	13 36 12.3 −80 19 07.9	92.2	483	9.7	tentative	18.21	−17.62
J1728-726	17 28 27.3 −72 37 36.9	94.7	214	6.8	good	18.67	−19.94
J1911-708	19 11 03.9 −70 48 25.9	25.9	238	7.0	good	20.45	−27.11
J1919-799	19 19 13.2 −79 59 07.0	276.6	1262	6.1	good	>22	−27.89
J1920-778	19 20 32.1 −77 53 44.2	46.8	108	5.9	none	–	−28.00
J1946-823	19 46 49.0 −82 22 53.7	35.9	219	8.6	tentative	19.98	−28.70
J1959-640	19 59 57.2 −64 02 06.1	239.0	475	5.3	tentative	20.50	−31.65
J2150-622	21 50 25.7 −62 10 13.5	83.4	230	5.3	tentative	15.85	−44.09
J2159-723	21 59 10.8 −72 19 13.1	19.6	142	10.5	good	16.61	−39.19
J2222-562	22 22 37.1 −56 17 33.5	121.5	190	5.6	good	18.69	−50.60
J2228-560	22 28 08.1 −56 00 02.2	48.2	163	5.5	good	17.53	−51.40
J2253-582	22 53 53.6 −58 13 10.5	99.0	242	4.6†	good	18.51	−52.75
J2336-818	23 36 17.0 −81 51 03.5	169.6	427	6.1	good	17.76	−34.81

†These sources had angular sizes less than 5 arcminutes. They are not included in any discussion involving physical properties.

Table B.2: Physical Properties for Candidates with $\theta > 5$' and Good Optical Identifications. Columns (5), (6) & (7) are for Ω_m = 1.0, Ω_Λ = 0 and H_0 = 50 kms^{-1}Mpc^{-1}. Columns (8) & (9) are for Ω_m = 0.3, Ω_Λ = 0.7 and H_0 = 70 kms^{-1}Mpc^{-1}.

(1) Source	(2) θ (arcmin)	(3) Int. S_{843} (mJy)	(4) z	(5) D (Mpc)	(6) log(P_{843}) (W/Hz)	(7) log(P_{325}) (W/Hz)	(8) D (Mpc)	(9) log(P_{843}) (W/Hz)
J0020-734	5.5	423	0.0839	0.70	25.12	25.45	0.52	24.86
J0129-646	5.4	362	0.1716	1.22	25.68	26.01	0.95	25.46
J0143-545	5.4	217	0.1791	1.26	25.50	25.83	0.99	25.28
J0237-645	7.3	145	0.4414	2.95	26.13	26.46	2.59	26.01
J0331-772	20.1	687	0.1487	4.09	25.83	26.16	3.15	25.61
J0400-849	7.0	175	0.1087	1.11	24.96	25.29	0.84	24.72
J0515-810	8.6	264	0.1020	1.29	25.09	25.42	0.97	24.84
J0843-701	5.0	203	0.1401	0.97	25.25	25.58	0.74	25.02
J1728-726	6.8	214	0.1792	1.59	25.49	25.82	1.24	25.28
J1911-708	7.0	238	0.3634	2.57	26.17	26.50	2.18	26.03
J1919-800	6.1	1262	0.3460	2.18	26.85	27.18	1.84	26.70
J2159-723	10.5	142	0.0974	1.52	24.78	25.11	1.14	24.53
J2222-563	5.6	190	0.1807	1.32	25.45	25.78	1.03	25.23
J2228-560	5.5	163	0.1140	0.91	24.97	25.31	0.69	24.73
J2336-819	6.1	427	0.1190	1.04	25.43	25.76	0.79	25.19

Table B.3: Physical Properties for Candidates with $\theta > 5$' and Tentative Optical Identifications. Columns (5), (6) & (7) are for Ω_m = 1.0, Ω_Λ = 0 and H_0 = 50 kms^{-1}Mpc^{-1}. Columns (8) & (9) are for Ω_m = 0.3, Ω_Λ = 0.7 and H_0 = 70 kms^{-1}Mpc^{-1}.

(1) Source	(2) θ (arcmin)	(3) Int. S_{843} (mJy)	(4) z	(5) D (Mpc)	(6) log(P_{843}) (W/Hz)	(7) log(P_{325}) (W/Hz)	(8) D (Mpc)	(9) log(P_{843}) (W/Hz)
J0047-831	6.4	543	0.3213	2.20	26.42	26.75	1.83	26.26
J0152-803	6.7	305	0.2730	2.09	26.02	26.35	1.70	25.84
J0631-541	5.9	694	0.1662	1.31	25.94	26.27	1.01	25.72
J0810-680	7.2	271	0.5092	3.10	26.53	26.86	2.79	26.44
J1259-776	5.9	439	0.1470	1.19	25.63	25.96	0.92	25.40
J1336-803	9.7	483	0.1493	1.98	25.68	26.02	1.52	25.46
J1946-824	8.6	219	0.3015	2.85	25.97	26.30	2.35	25.80
J1959-640	5.3	475	0.3707	1.97	26.49	26.82	1.67	26.35
J2150-622	5.3	230	0.0585	0.49	24.54	24.87	0.36	24.27

Appendix C

Images of the GRG Candidates

The following are SUMSS contours on Digitised Sky Survey Epoch 2 greyscale images for all the candidate sources.

Contours are set at 3, 5, 7, 10, 15, 20, 30, 50, 70, 100, 150, 200 mJy/beam unless otherwise stated.

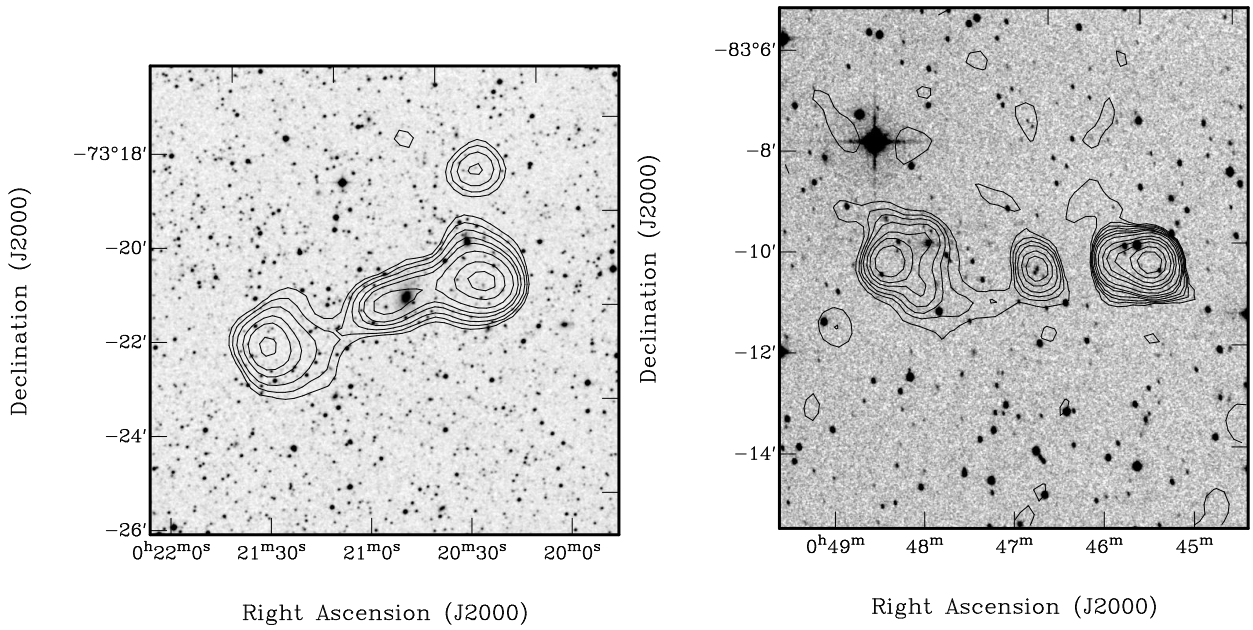

Figure C.1: J0020-733 (left) and J0047-831 (right). Contours for J0020-733 are set at 5, 7, 10, 15, 20, 30, 50, 70 mJy/beam.

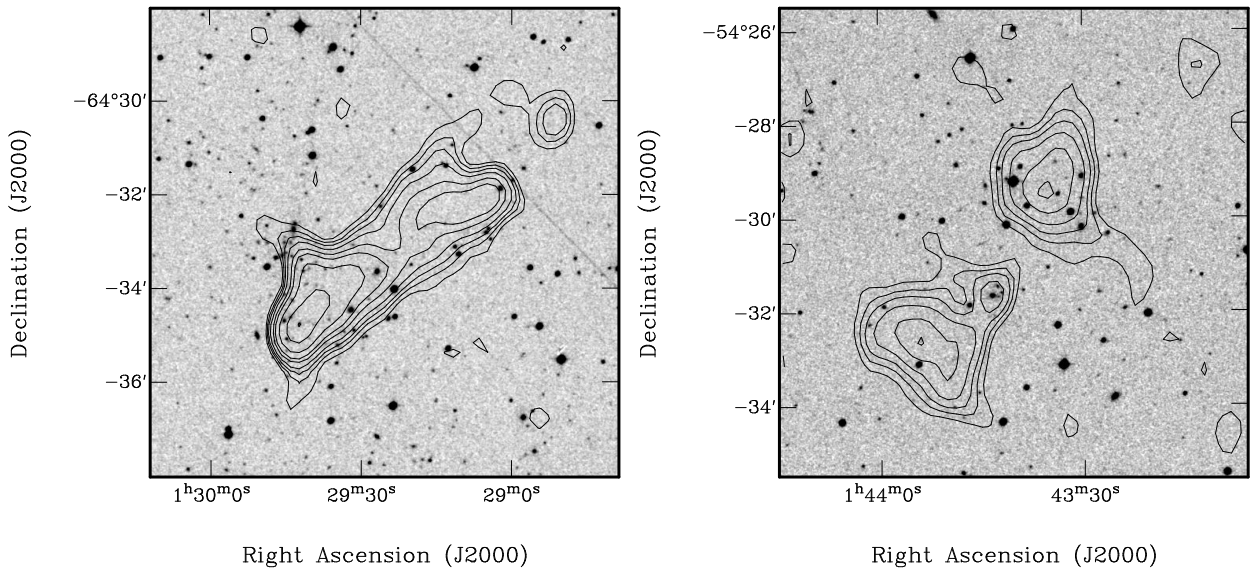

Figure C.2: J0129-645 (left) and J0143-545 (right).

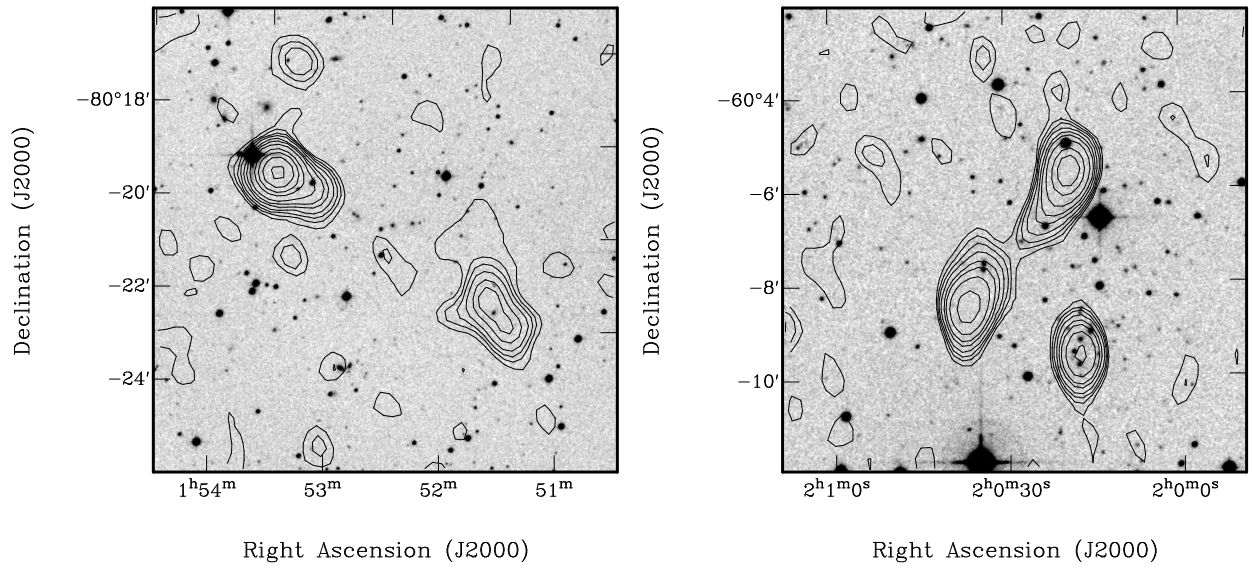

Figure C.3: J0152-803 (left) and J0200-601 (right).

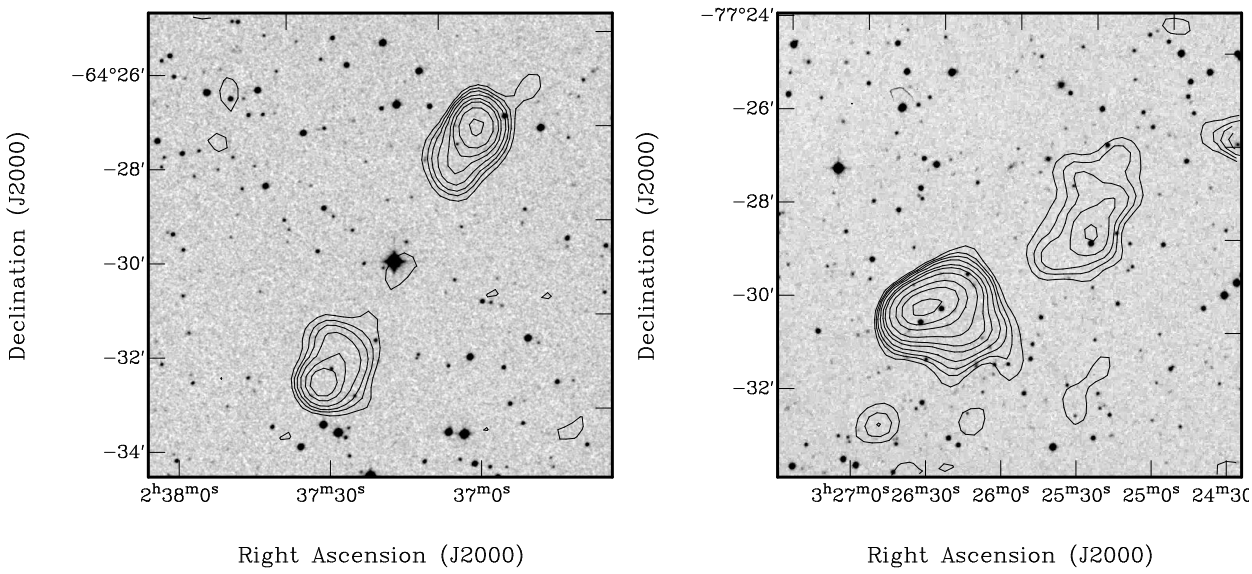

Figure C.4: J0237-644 (left) and J0326-775 (right).

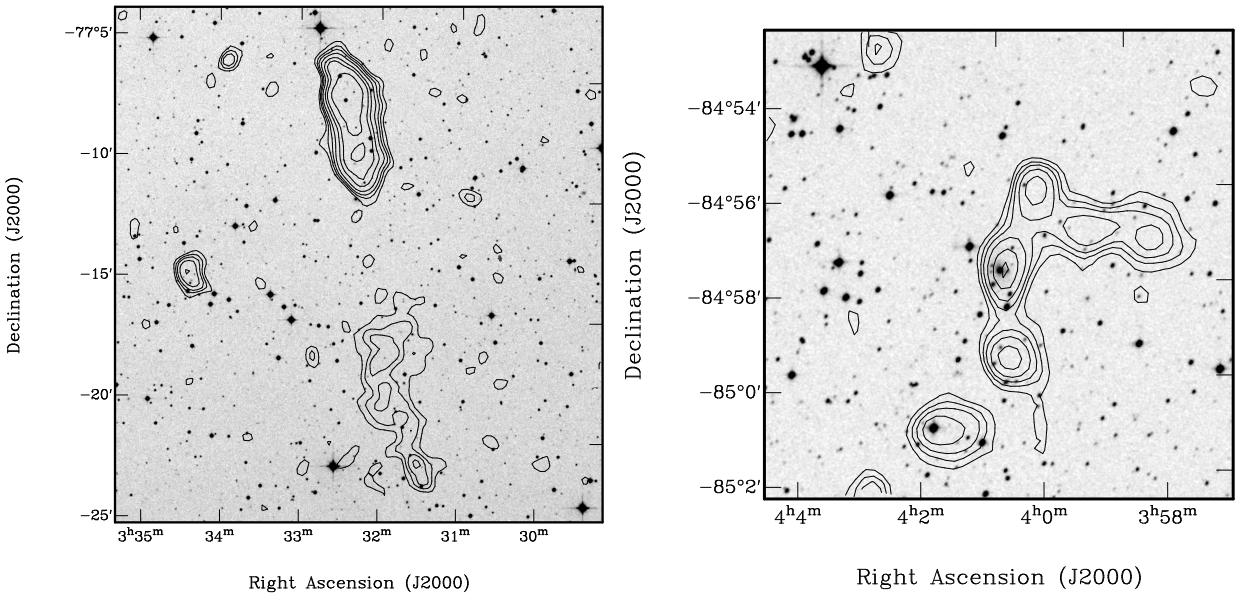

Figure C.5: J0331-771 (left) and J0400-849 (right).

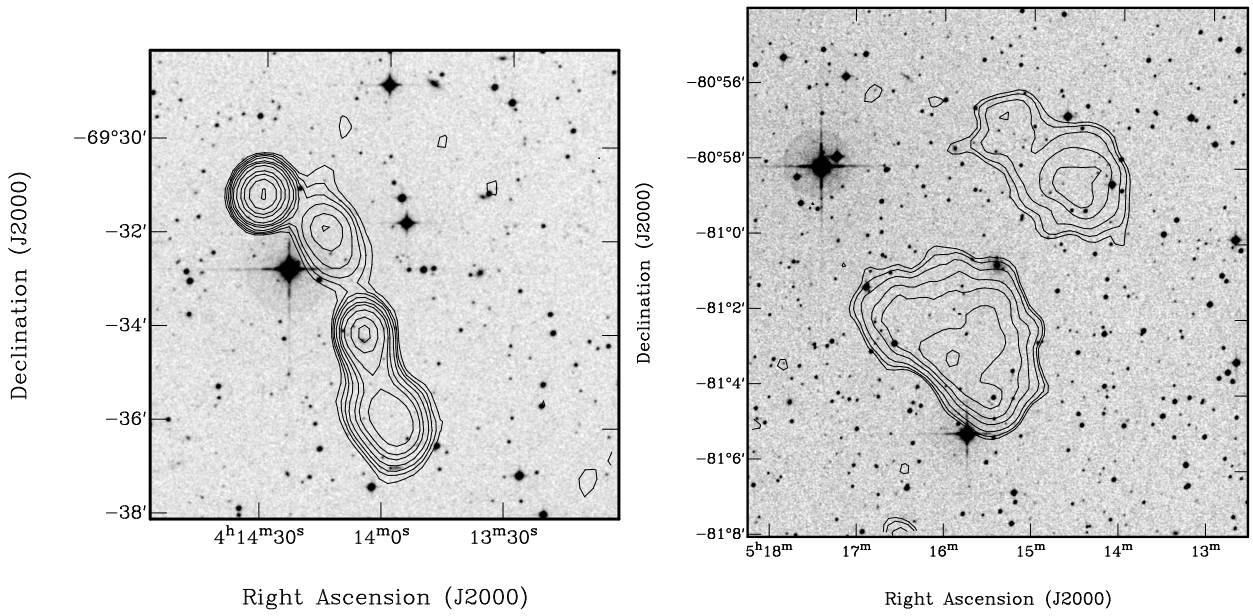

Figure C.6: J0414-695 (left) and J0515-810 (right). Contours for J0515-810 are set at 1.5, 2, 3, 5, 7, 10, 15 mJy/beam.

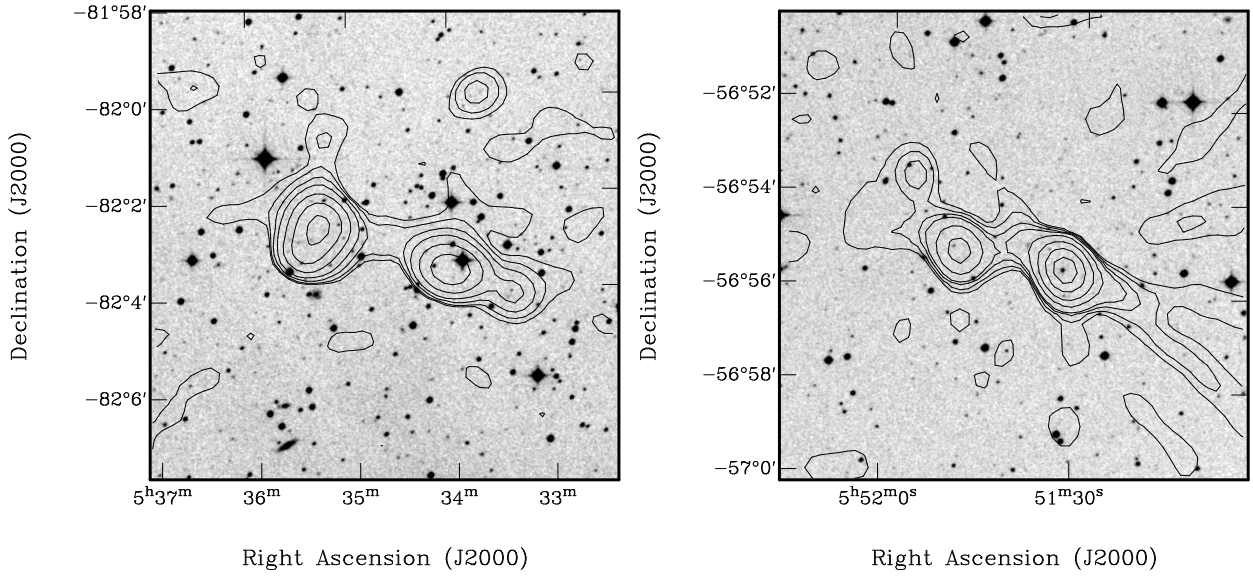

Figure C.7: J0534-821 (left) and J0551-569 (right). Contours for J0534-821 are set at 3, 7, 15, 30, 70, 150, 300 mJy/beam. Contours for J0551-569 are set at 3, 10, 20, 30, 70, 150, 300, 500 mJy/beam.

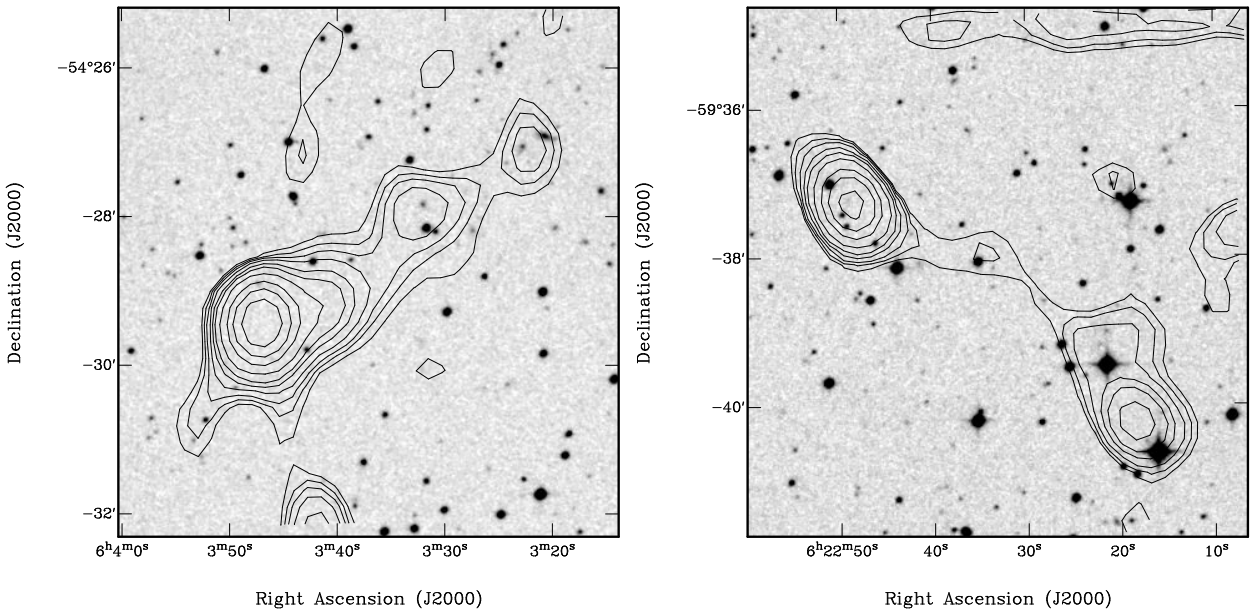

Figure C.8: J0603-544 (left) and J0622-596 (right). Contours for J0622-596 are set at 5, 7, 10, 15, 20, 30, 50, 70, 100 mJy/beam.

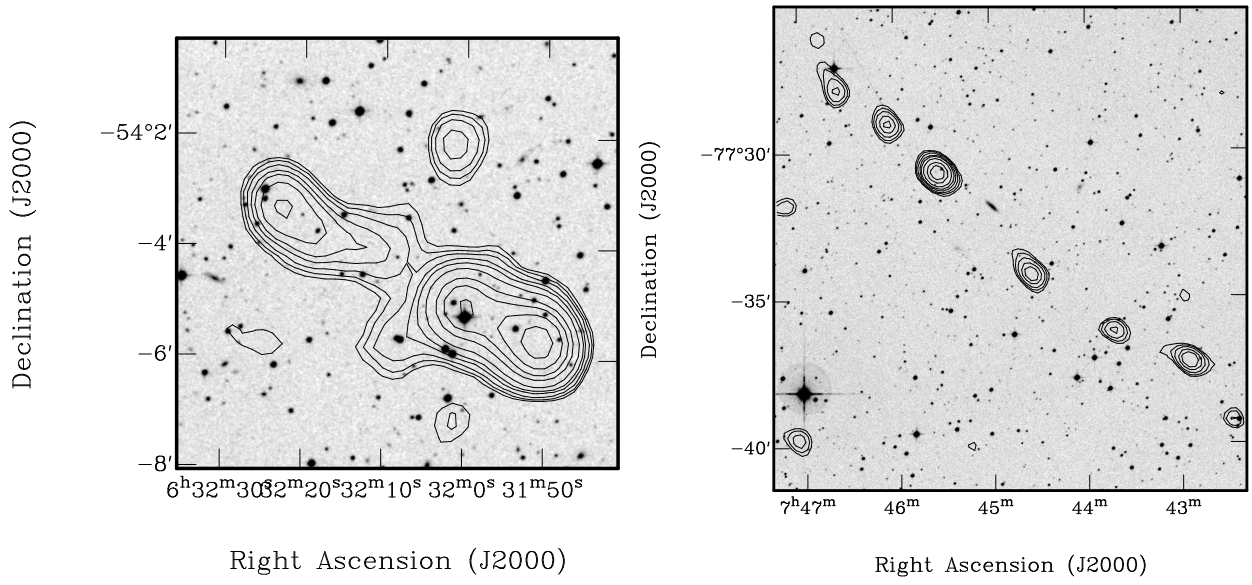

Figure C.9: J0631-540 (left) and J0745-775 (right). Contours for J0631-540 are set at 5, 7, 10, 15, 20, 30, 50, 70, 100, 150 mJy/beam. Contours for J0745-775 are set at 5, 7, 10, 15, 20, 30, 50, 70 mJy/beam

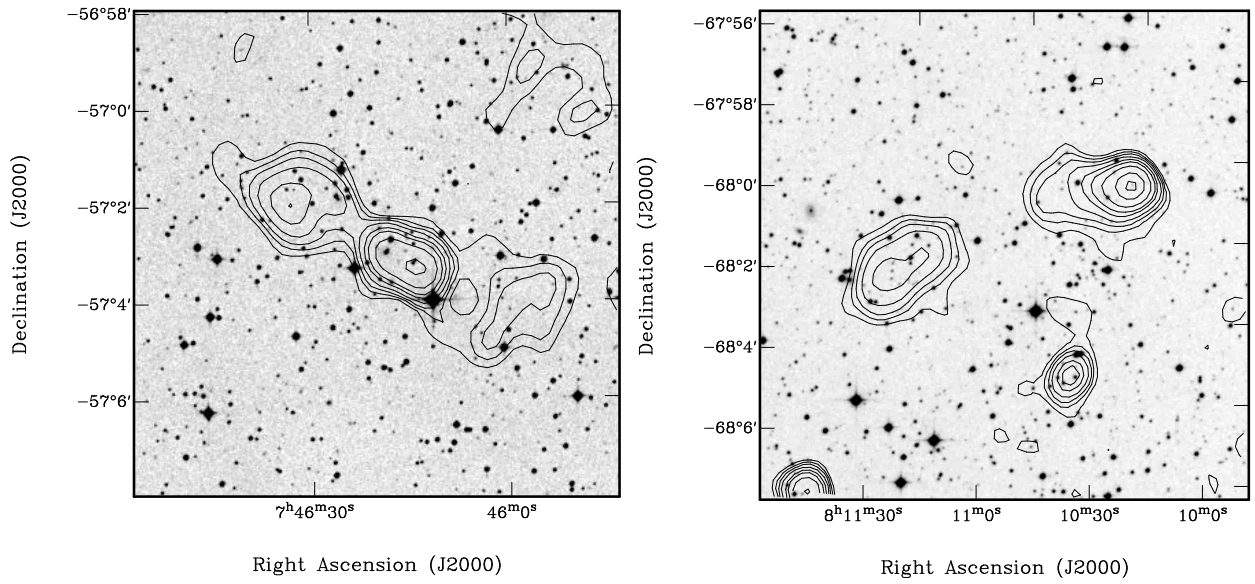

Figure C.10: J0746-570 (left) and J0810-680 (right). The optical field for J0746-570 is DSS Epoch 1, because Epoch 2 had image artifacts.

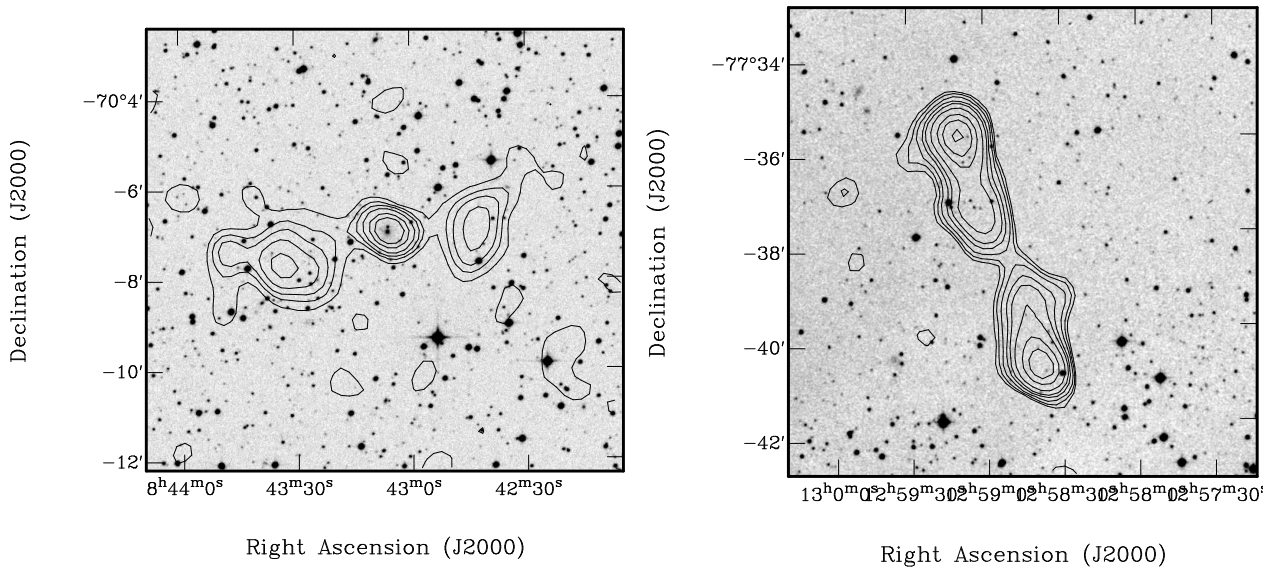

Figure C.11: J0843-701 (left) and J1259-776 (right). Contours for J1259-776 are set at 5, 7, 10, 15, 20, 30, 50, 70, 100 mJy/beam.

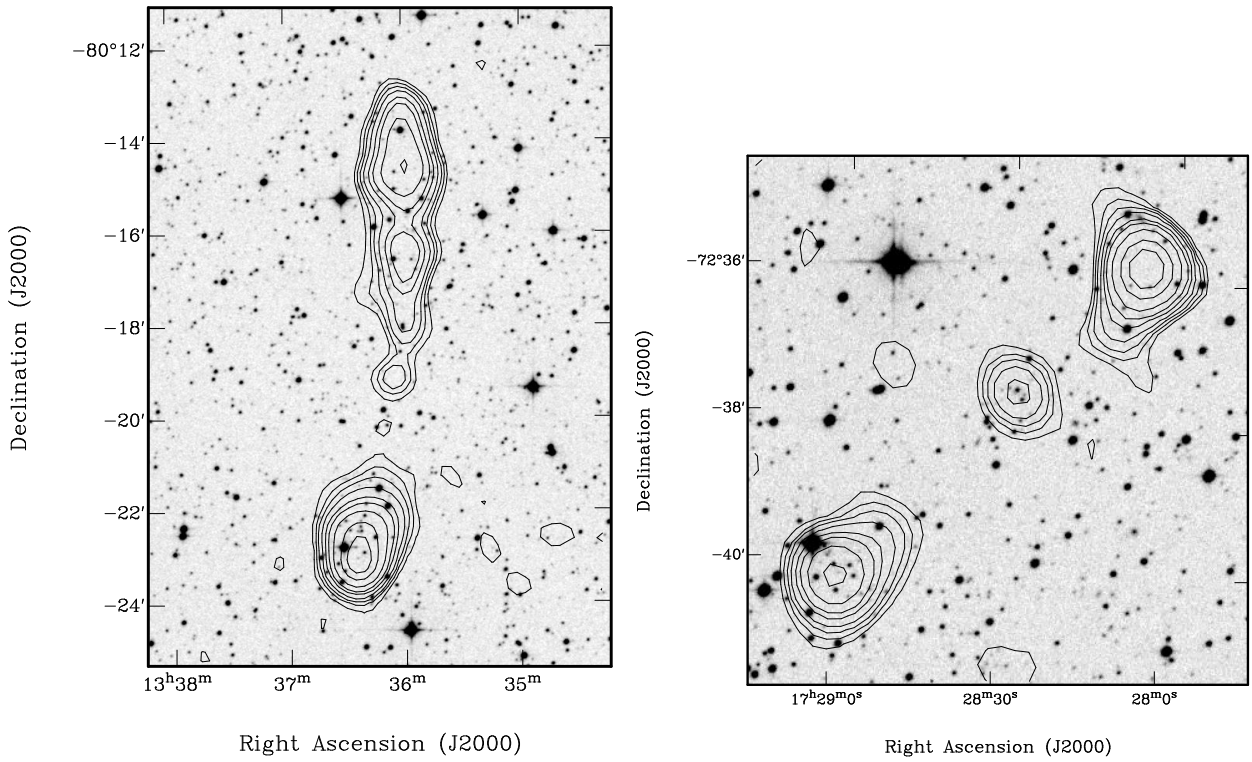

Figure C.12: J1336-803 (left) and J1728-726 (right).

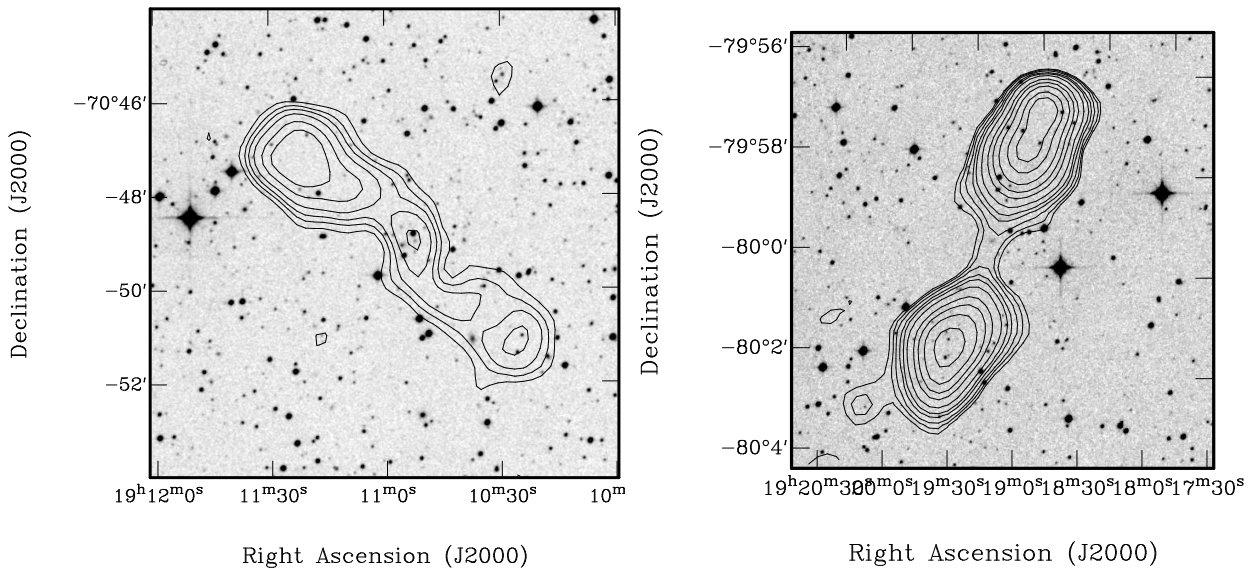

Figure C.13: J1911-708 (left) and J1919-799 (right). Contours for J1919-799 are set at 5, 7, 10, 15, 20, 30, 50, 70, 100, 150, 200 mJy/beam.

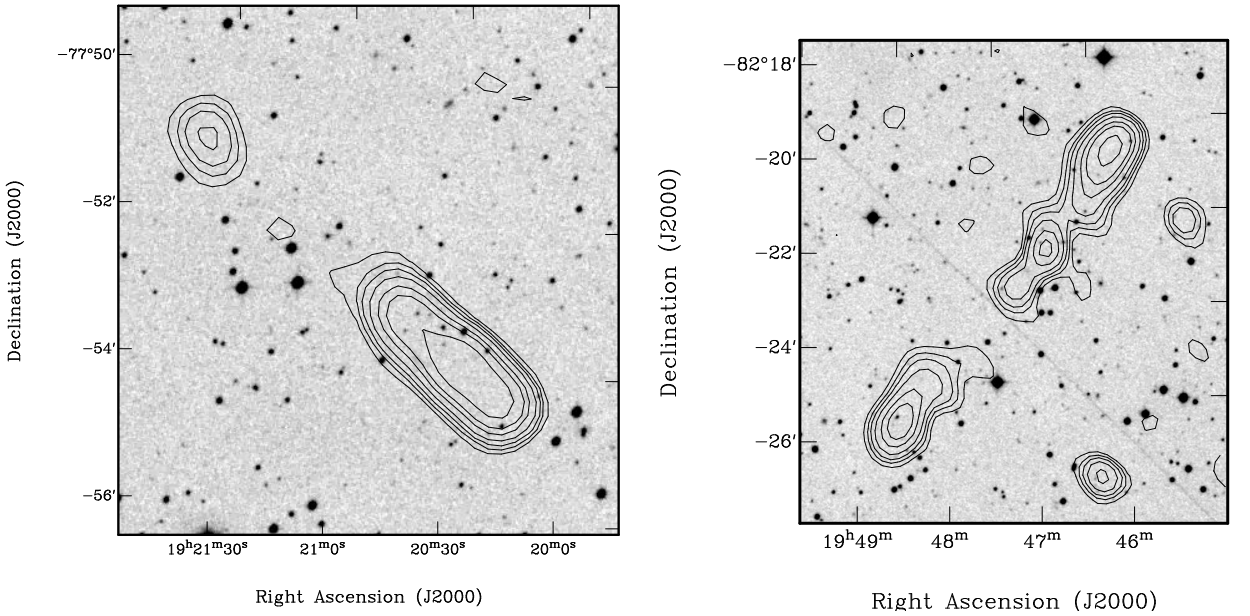

Figure C.14: J1920-778 (left) and J1946-823 (right).

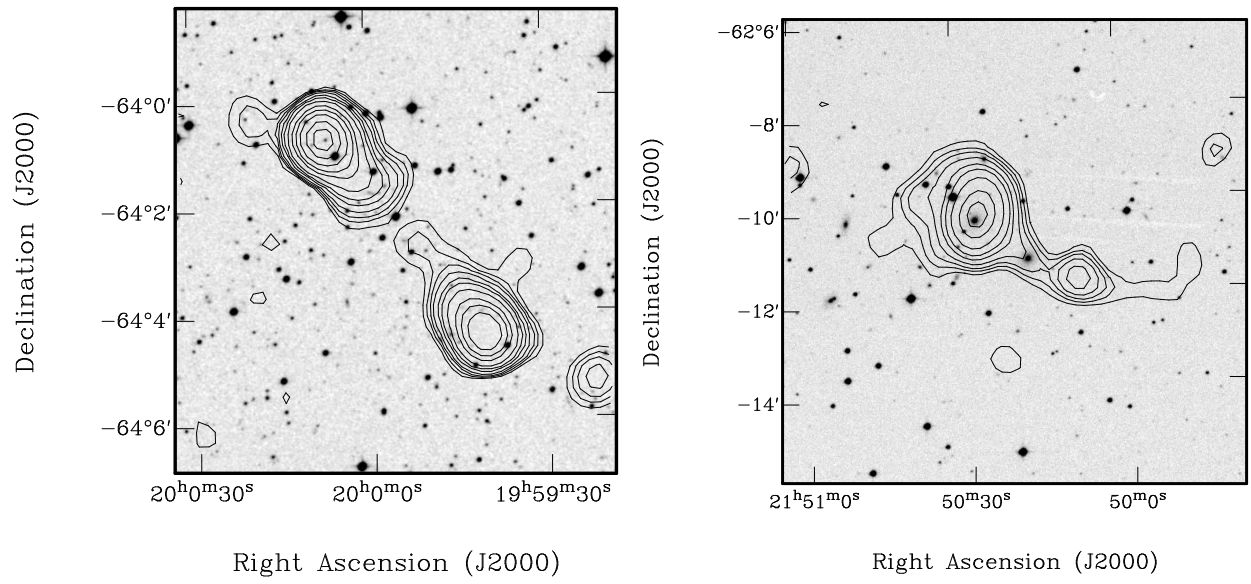

Figure C.15: J1959-640 (left) and J2150-622 (right).

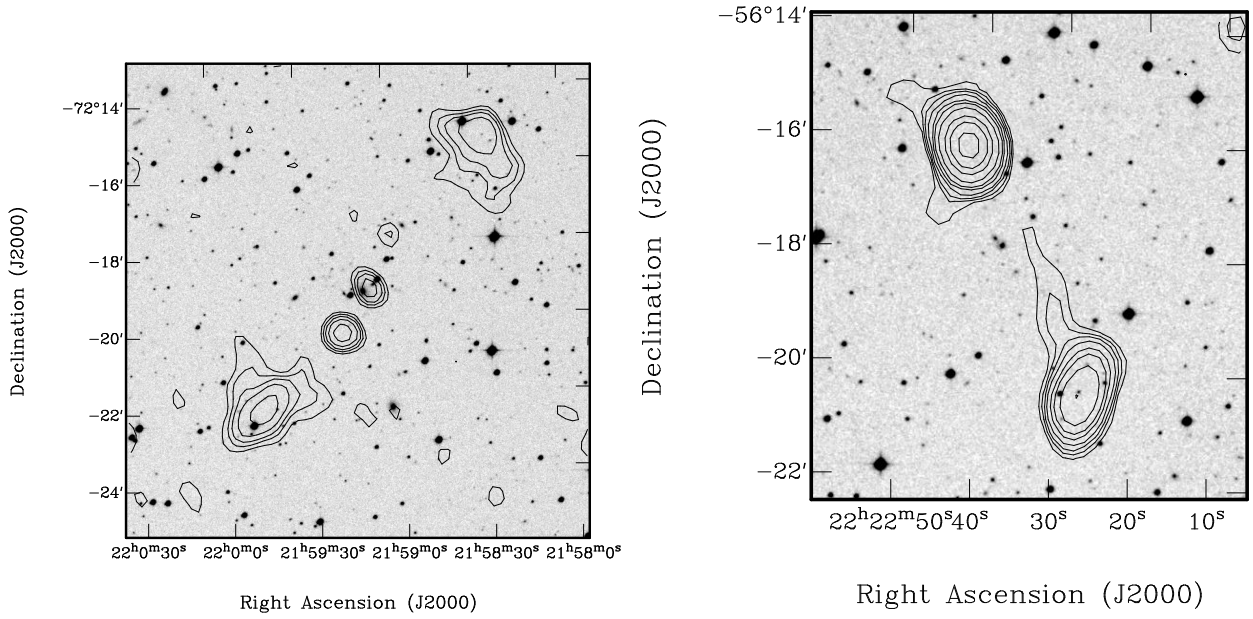

Figure C.16: J2159-723 (left) and J2222-562 (right).

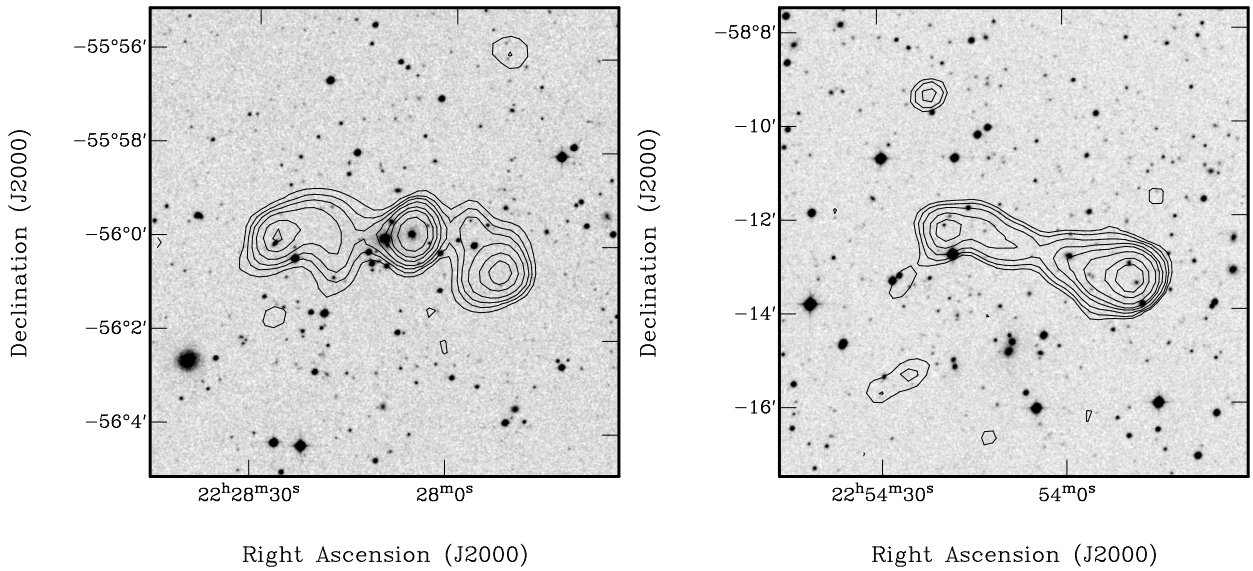

Figure C.17: J2228-560 (left) and J2253-582 (right). Contours for J2253-582 are set at 5, 7, 10, 15, 20, 30, 50, 70 mJy/beam.

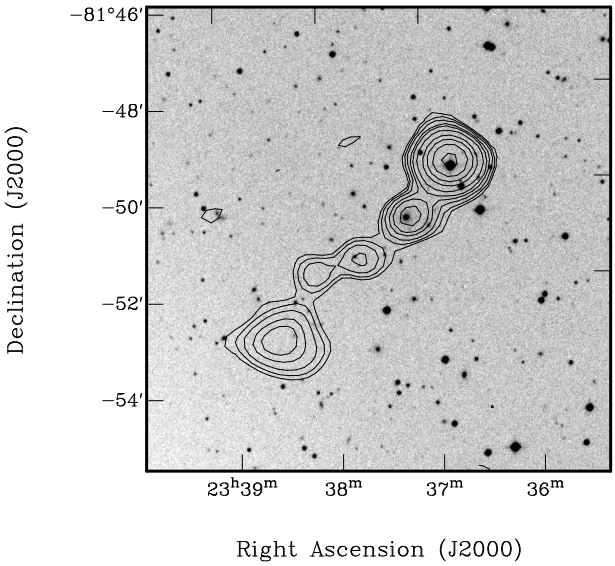

Figure C.18: J2336-818. Contours for J2336-818 are set at 5, 7, 10, 15, 20, 30, 50, 70, 100, 150 mJy/beam.

Appendix D

Calculation of Physical Properties

The linear size of a source is calculated using the formula:

$$D = \frac{\theta}{(1+z)^2}\, D_L \tag{D.1}$$

where D is the linear size in Mpc, θ is the angular size in radians, z is the redshift and D_L is the luminosity distance in Mpc.
The radio power is calculated using the formula:

$$P_{em} = 4\pi \times 10^{-26}\, S_{obs}\, D_L^2\, (1+z)^{-(1+\alpha)}\, (\frac{\nu_{em}}{\nu_{obs}})^{\alpha} \tag{D.2}$$

where P_{em} is the emitted radio power in W/Hz at frequency ν_{em}, S_{obs} is the total flux in Jy observed at frequency ν_{obs}, z is the redshift, D_L is the luminosity distance in metres and α is the spectral index defined by $S_\alpha \propto \nu^\alpha$.

D.1 Luminosity Distance and Cosmology

The definition of the luminosity distance D_L is dependent on cosmological assumptions, specifically the density of matter as a fraction of critical density, Ω_m, the cosmological constant as a fraction of critical density, Ω_Λ, the deceleration paramater $q_0 = \frac{1}{2}\Omega_m - \Omega_\Lambda$ and the Hubble constant, H_0.

For a universe with no cosmological constant, Ω_Λ = 0, the luminosity distance is defined by (McVittie, 1965):

$$D_L = \frac{c}{H_0 q_0^2}(q_0 z + (q_0 - 1)(\sqrt{1+2q_0 z} - 1)) \tag{D.3}$$

where c is the speed of light. A special case is the Einstein-de Sitter universe with Ω_m = 1, q_0 = 0.5. For this model the luminosity distance is:

$$D_L = \frac{c}{H_0}\, 2(1 + z - (\sqrt{1+z})) \tag{D.4}$$

A general power series approximation for the luminosity distance, useful for the case of a nonzero cosmological constant, is (White, 1999):

$$D_L = \frac{c}{H_0}\,(1+z)\int_0^z \frac{dx}{(1+x)(1+q_0 x)} \approx \frac{cz}{H_0}(1 + \frac{1-q_0}{2}\, z + \frac{2q_0^2 - q_0 - 1}{6}\, z^2) \tag{D.5}$$

Note that the dimensions of D_L are determined by the dimensions used for c and H_0. For D_L in Mpc use c in kms^{-1} and H_0 in kms^{-1}Mpc^{-1}. For D_L in m use c in ms^{-1} and H_0 in s^{-1}.